ADAPTATION OF COLON CANCER CELLS TO HISTONE DEACETYLASE INHIBITORS GENERATES CELL LINES WITH A NON-MALIGNANT PHENOTYPE

by

DIANA S VENGSARKAR

A thesis submitted to the

Graduate School-New Brunswick

and

The Graduate School of Biomedical Sciences

Rutgers, The State University of New Jersey

In partial fulfillment of the requirements

For the degree of

Master of Science

Graduate Program in Microbiology and Molecular Genetics

Written under the direction of

Arnold B. Rabson, MD

And approved by

_____

_____

_____

New Brunswick, New Jersey

May 2016

ABSTRACT OF THE THESIS

ADAPTATION OF COLON CANCER CELLS TO HISTONE DEACETYLASE INHIBITORS GENERATES CELL LINES WITH A NON-MALIGNANT PHENOTYPE

by DIANA S VENGSARKAR

Thesis Director:

Arnold B. Rabson, MD

Histones are subject to various covalent post-translational modifications that can influence specific changes in chromatin structure and levels of transcription. The Polycomb (PcG) and Trithorax (TrxG) group systems are classic epigenetic systems that mediate transcriptional repression and activation, respectively, through mutually-exclusive modifications of histone H3 at lysine 27 (H3K27) in the gene promoter region. The Polycomb Repressive Complex 2 (PRC2) mediates transcriptional silencing by trimethylating H3K27 while TrxG proteins mediate transcriptional activation by acetylating H3K27. Histone deacetylases (HDACs) 1 and 2 are associated with the PRC2 complex and their overexpression has been linked to a variety of cancers.

The Rabson Laboratory adapted SW480 colon cancer cells to the pan-HDAC inhibitor vorinostat. Vorinostat-adapted cells (SH80) showed a near elimination of tumorigenicity in tumor xenografts, global changes in mRNA expression, and an upregulation of PRC2 target genes. The overarching goal of this research was to determine which changes were necessary to generate the non-malignant phenotype of SH80. First, we used H3K27 trimethylation and acetylation status to evaluate changes at PRC2 targets as a function of i) vorinostat concentration and ii)

acute treatment versus adaptation with vorinostat. Second, we investigated if selective inhibition of HDACs 1, 2, and 3 would be sufficient to generate the non-malignant phenotype by adapting SW480 cells to the inhibitor CI-994 and evaluating changes in proliferation, colony formation, and gene expression at PRC2 targets.

Three PRC2 target genes were identified that had striking changes in mRNA expression as a function of vorinostat concentration and/or adaptation that correlated with H3K27 modifications and may be important to generating the non-malignant phenotype: *TSPAN8*, *STMN2*, and *EDN3*. Cells adapted to 12 μM CI-994 showed a substantial reduction in colony formation, suggesting that targeted inhibition of HDACs 1, 2, and 3 may reduce tumorigenicity. Changes in mRNA expression in CI-994 adapted cells were similar to SH80 cells, indicating that inhibition of HDACs 1, 2, and 3 leads to altered expression of PRC target genes. Substantial changes in gene expression were observed for *TSPAN8*, *STMN2*, and *EDN3*, further reinforcing the idea that these genes may be of particular importance to the non-malignant phenotype.

Acknowledgements

I would like to express my deepest appreciation to my advisor Dr. Arnold Rabson for his guidance and patience throughout this research program. He created a supportive environment at the Child Health Institute which enabled the exploration of new ideas described in this thesis and continually prodded me in new directions as the research evolved.

I would like to thank my committee members Dr. Kathleen Scotto and Dr. Dan Medina for reviewing my results and suggesting modifications, which led to an improved body of work.

A special thanks to Dr. Hsin-Ching Lin for her wisdom and support throughout my tenure at the Rabson Lab. Cindy was a sounding board, a patient ear and a friend who helped me understand the prior work in this field, and with whom I could bounce ideas during the research. In addition, a thank you to my colleagues at the Rabson Lab, past and present, Celine Granier, Tiffany Tsang, Elizabeth Isaac, George Wei, and Reid Singer for creating a positive and collaborative atmosphere in the lab.

Looking back at my experience at Rutgers, I am grateful to my fellow General Biology compatriots Dr. Gregg Transue, Dr. Monica Torres, Dr. Andrew Vershon, Hillary Stires, David Jespersen, and George Condon, for a mentally stimulating experience developing the new Biological Research Laboratory course. Also, my heartfelt thanks to Dr. Nilgun Tumer and Dr. Michael Pierce for providing an undergraduate research experience that created a strong foundation for my graduate studies.

Table of Contents

List of Tables

List of Figures

Chapter 1: Introduction

1.1 Epigenetics and the Histone Code

Chromatin is the complex of DNA and proteins that provides the means for packaging DNA within the nucleus of the cell (Dawson and Kouzarides, 2012). The fundamental unit of chromatin is the nucleosome which consists of a histone octamer with 147 base pairs of DNA wrapped around it. Each histone octamer is composed of two units each of four core histone proteins H2A, H2B, H3, and H4. Research and new technologies have significantly advanced the understanding of chromatin regulation through mechanisms such as DNA modifications, histone modifications, and non-coding RNAs (Dawson and Kouzarides, 2012; Füllgrabe *et al*., 2011). This has led to a re-evaluation of how epigenetics is defined. A consensus definition for an epigenetic trait has been proposed as "a stably heritable phenotype resulting from changes in a chromosome without alterations in the DNA sequence", with heritability through either meiosis or mitosis (Berger *et al*., 2009). However, broader definitions have been proposed in order to include transient histone modifications involved in processes such as transcriptional regulation, DNA replication, and DNA repair. One such proposal defined epigenetics as "the structural adaptation of chromosomal regions so as to register, signal, or perpetuate altered activity states" (Bird, 2007).

Histones are subject to various covalent post-translational modifications (PTMs) at specific amino acid residues in the globular domains and the unstructured amino- and carboxy-terminal tails (Berger, 2007; Kouzarides, 2007). However, the amino-terminal tail contains the highest density of PTM targets (Oliver and Denu, 2011). There are at least 16 different classes of histone modifications including acetylated lysine, methylated lysine and arginine, ubiquitylated lysine, and phosphorylated serine, threonine, and tyrosine (Dawson and Kouzarides, 2012).

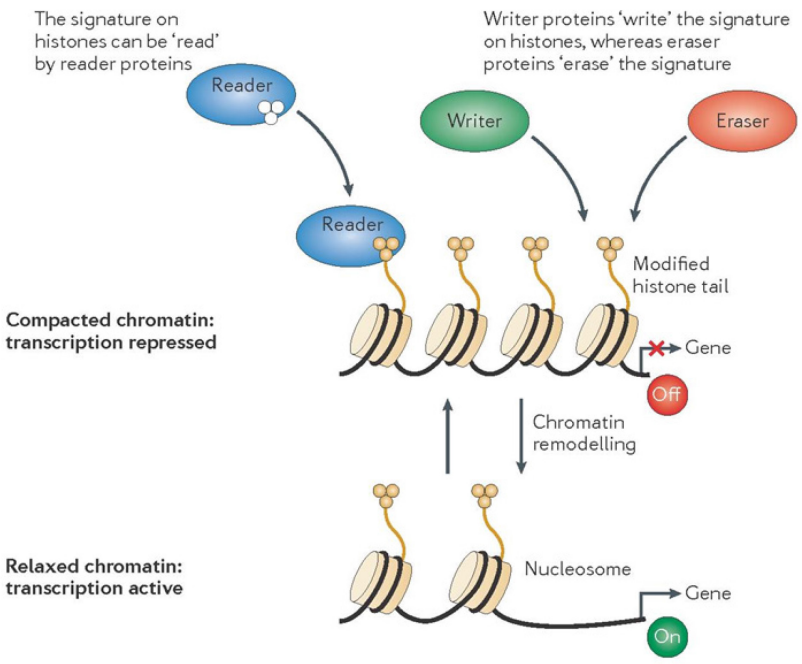

Figure 1. Readers, writers, and erasers regulate chromatin structure and transcription (Højfeldt et al., 2013).

The histone code is a hypothesis that different combinations of histone PTMs influence specific changes in chromatin structure and levels of transcription. PTMs can directly cause structural changes in chromatin, such as chromatin compaction or relaxation, by altering the electrostatic charge of the histone (Füllgrabe *et al*., 2011). PTMs also act indirectly on chromatin by serving as binding sites for reader proteins (Figure 1) (Oliver and Denu, 2011). Reader proteins contain domains that specifically bind histone PTMs, such as bromodomains that recognize acetylated lysines or chromodomains that recognize methylated lysines (Füllgrabe *et al*., 2011). Readers recruit other protein complexes that catalyze additional chromatin modifications or DNA-templated processes such as transcription (Oliver and Denu, 2011). Writer proteins, such as histone methyltransferases (HMTs) and histone acetyltransferases (HATs), are enzymes that catalyze the addition of PTMs. Eraser proteins, such as histone demethylases (HDMs) and

histone deacetylases (HDACs), are enzymes that remove histone PTMs (Füllgrabe *et al*., 2011; Højfeldt *et al*., 2013).

Histone PTMs have different effects on transcription depending on the class of modification and the position of the modified residue (Table 1). Additionally, lysine and arginine can undergo mono-, di-, or trimethylation, with each modification being functionally distinct. For example, trimethylation of lysine 4 in histone H3 (H3K4me3) near the gene promoter region is associated with transcriptional activation (Berger, 2007).

Table 1. Sites of histone PTMs and their role in transcription (Berger, 2007).

Histone PTMs		
Acetylated lysine (Kac)	H3 (9, 14, 18, 56), H4 (5, 8, 13, 16), H2A, H2B	Activation
Phosphorylated serine/ threonine (S/Tph)	H3 (3, 10, 28), H2A, H2B	Activation
Methylated arginine (Rme)	H3 (17, 23), H4 (3)	Activation
Methylated lysine (Kme)	H3 (4, 36, 79) H3 (9, 27), H4 (20)	Activation Repression
Ubiquitylated lysine (Kub)	H2B (123§/120¶) H2A (119¶)	Activation Repression
Sumoylated lysine (Ksu)	H2B (6/7), H2A (126)	Repression
Isomerized proline (Pisom)	H3 (30–38)	Activation/ repression

1.2 Polycomb and Trithorax Group Systems

The Polycomb and Trithorax group systems are classic epigenetic systems that mediate transcriptional repression and activation, respectively. These systems were discovered and have been studied most extensively in *Drosophila melanogaster*. Trithorax group (TrxG) proteins and Polycomb group (PcG) proteins are components of multi-protein complexes with reader, writer,

and eraser functions. TrxG proteins work antagonistically to PcG proteins in controlling the expression of the same target genes through histone PTMs (Kolybaba and Classen, 2014).

In Polycomb-mediated silencing, histone H3 is trimethylated at lysine 27 (H3K27me3) by Polycomb Repressive Complex 2 (PRC2) in the gene promoter region (Figure 2). Polycomb Repressive Complex 1 (PRC1) binds H3K27me3 and catalyzes the ubiquitylation of lysine 119 on histone 2A. H2AK119ub can induce chromatin compaction and may inhibit transcriptional elongation by RNA polymerase II (Schuettengruber *et al*., 2011).

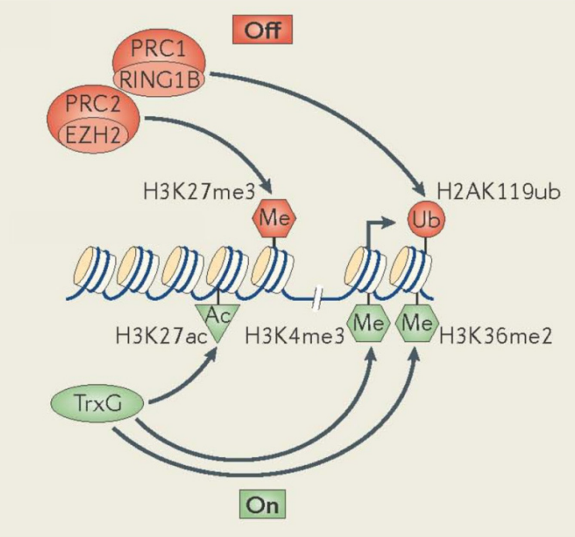

Figure 2. The antagonistic interactions of PcG and TrxG proteins mediate transcriptional silencing and activation, respectively (Schuettengruber *et al*., 2011).

The PRC2 complex contains four core components: enhancer of zeste homolog 2 (EZH2), suppressor of zeste homolog 12 (SUZ12), embryonic ectoderm development (EED), and retinoblastoma-binding protein 4 or 7 (RBBP4 or RBBP7) (Figure 3A). EZH2 is an HMT that catalyzes H3K27 di- and tri-methylation via its SET domain. SUZ12 and EED are required for the HMT activity of EZH2 (Mills, 2010). RBBP4 and 7 are histone binding proteins, but they are not essential to the HMT activity of PRC2 (Morey and Helin, 2010). HDACs 1 and 2 have been shown to co-immunoprecipitate with EED and EZH2, suggesting they are recruited by the PRC2 complex to remove the acetyl group from H3K27 (van der Vlag and Otte, 1999).

PRC1 complexes have multiple forms which contain four core components: a chromobox homolog protein (CBX2, 7, or 8), a polyhomeotic homolog (PHC1, 2, or 3), BMI1, and ring finger protein 1 or 2 (RING1A or 1B). PRC1 binds the H3K27me3 mark through the chromodomain of CBX proteins and catalyzes ubiquitylation of H2AK119 through the RING protein subunit. BMI1 is required for RING1B E3 ubiquitin ligase activity, which is responsible for the majority of H2AK119 ubiquitylation (Morey and Helin, 2010).

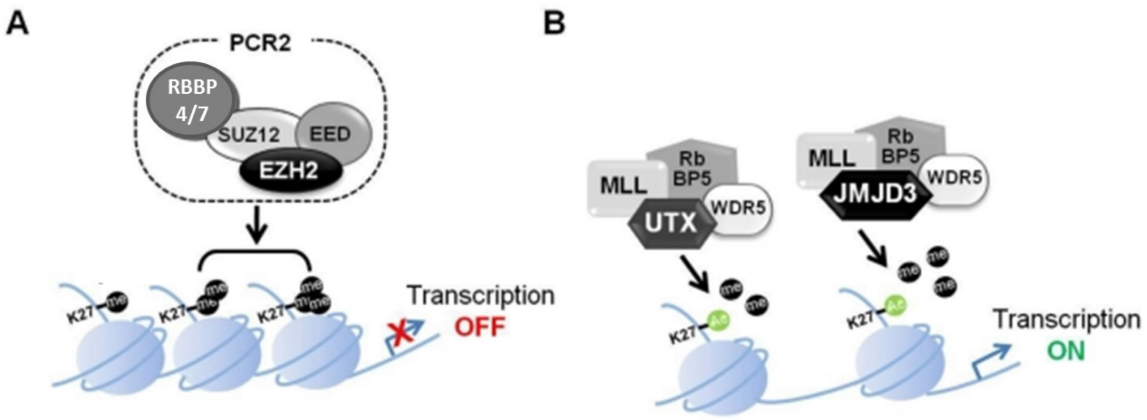

Figure 3. PcG and TrxG protein-containing complexes that modify H3K27. (A)The core components of the PRC2 complex that di- and tri-methylate H3K27, leading to transcriptional repression. (B) MLL protein-containing complexes that remove di- and tri-methylation on H3K27, leading to H3K27ac and transcriptional activation (adapted from Yoo and Hennighausen, 2012).

In Trithorax-mediated activation, histone H3 is dimethylated at lysine 36 and trimethylated at lysine 4 by TrxG proteins in the gene promoter region (Figure 2) (Schuettengruber *et al*., 2011). TrxG proteins interact with the HAT CREB-binding protein (CBP), which catalyzes the acetylation of H3K27 (H3K27ac). H3K36me2 and H3K4me3 inhibit PRC2-mediated silencing while the acetylation and trimethylation modifications of H3K27 are mutually exclusive. H3K27ac neutralizes the positive charge of lysine, which promotes an open chromatin configuration due to a reduction in the electrostatic histone-DNA interactions (Steffen and Ringrose, 2014).

The Mixed-Lineage Leukemia (MLL) protein-containing complexes from the Trithorax group consist of five core components: an MLL protein (MLL 1, 2, 3, or 4), WD repeat domain 5 (WDR5), retinoblastoma-binding protein 5 (RBBP5), dumpy 30 homolog (DPY30), and absent small and homeotic disks 2 homolog (ASH2L). MLL proteins have a conserved SET domain that catalyzes mono-, di-, or tri-methylation of H3K4, with different MLL-containing complexes targeting different gene loci (Smith *et al*., 2011). All of the core components are required for HMT activity (Ullius *et al*., 2014). MLL1 and MLL2-containing complexes mediate trimethylation of H3K4 at PcG target gene promoters. MLL3 and MLL4-containing complexes mediate monomethylation of H3K4 at enhancer regions (Kolybaba and Classen, 2014). They also contain the HDMs UTX (aka KDM6A) or JMJD3 (aka KDM6B) which remove the di- and tri-methylation mark on H3K27, allowing for H3K27 acetylation by the HATs CBP or P300 (Figure 3B) (Yoo and Hennighausen, 2012). The TrxG protein BRD4 (bromodomain-containing 4) binds H3K27ac and phosphorylates serine 2 in the C-terminal domain of RNA polymerase II, which promotes transcriptional elongation (Steffen and Ringrose, 2014).

Activating methylation marks on H3K4 are removed by two classes of HDMs. The LSD family (LSD1 and 2) can demethylate mono- and di-methylated lysines while a subset of the Jumonji C domain-containing demethylases (KDM5A, 5B, 5C, and 5D) demethylate di- and tri-methylated H3K4 (Højfeldt *et al*., 2013).

1.3 Involvement of PcG and TrxG Systems in Cancer

An initial theory in human cancer research was that gain of PcG activity or loss of TrxG activity leads to hypermethylation of H3K27 and epigenetic silencing of tumor suppressor genes. However, it has been shown that loss of PcG activity or gain TrxG activity can lead to aberrant

expression of genes linked to carcinogenesis. Thus, a newer model has emerged that cancer can be caused by an imbalance between the PcG and TrxG systems through the activation of oncogenes, inactivation of tumor suppressor genes, or the reactivation of stem cell-associated genes (Mills, 2010). A review of writer and eraser proteins in the PcG and TrxG systems, and their involvement in carcinogenesis, is summarized below.

Histone methyltransferases EZH2 and MLL proteins have been implicated in cancer. Progression and invasion was associated with overexpression of EZH2 in a wide range of hematological and solid malignancies (Hock, 2012). Upregulation of EZH2 correlated with a poor prognosis in prostate and breast cancer. Heterozygous tyrosine 641 mutations in the EZH2 SET domain conferred increased catalytic activity in diffuse large B cell lymphoma (DLBCL). Conversely, EZH2 inactivating mutations or deletions were reported in myeloid malignancies. Loss-of-function mutations in MLL2 and 3 have been associated with a variety of cancers. It was also shown that chromosomal translocations produced MLL1 fusion proteins with oncogenic activity in acute myeloid leukemia (AML) and acute lymphoid leukemia (ALL) (Dawson and Kouzarides, 2012).

Histone acetyltransferases linked to cancer include the TrxG-associated proteins CBP and P300. Inactivating mutations in CBP and P300 have been found in AML, ALL, and DLBCL. In addition, mutations in P300 have also been found in colorectal, breast, and pancreatic cancers (Dawson and Kouzarides, 2012). MLL fusions with CBP and P300 have occurred in therapy-induced secondary leukemia (Iyer *et al*., 2004).

Histone demethylases that act aberrantly on H3K4 and H3K27 have been associated with a diverse range of cancers. Overexpression of LSD1 has been shown in lung, bladder, and

colorectal carcinoma. LSD1 was upregulated in neuroblastoma and correlated with a poor prognosis. KDM5A fusion to nucleoporin-98 has been reported in AML. Overexpression of KDM5B has been shown to lead to repression of tumor suppressor genes such as BRCA1 in breast cancer. Loss-of-function mutations in the TrxG protein UTX have been reported in multiple myeloma as well as other cancers. Upregulation of JMJD3 has been found in prostate cancer and Hodgkin's lymphoma (Füllgrabe *et al*., 2011).

Histone deacetylases associated with the PRC2 complex have been linked to variety of cancers. Overexpression of HDAC1 has been found in colon, gastric, prostate, and breast cancer. Similarly, overexpression of HDAC2 has been reported in colorectal, gastric, and cervical cancer. Additionally, upregulation of HDAC3 has been shown in colon cancer (Bolden *et al*., 2006).

1.4 Histone Deacetylases and Types of Inhibitors

Histone deacetylases (HDACs) are lysine deacetylases that act on both histone and non-histone proteins. HDACs are components of multi-subunit complexes that largely influence the enzymatic target (Dawson and Kouzarides, 2012). Human HDACs have been grouped into four classes based on their enzymatic activities, subcellular location, and homology to yeast HDACs (Figure 4) (Bolden *et al*., 2006). HDAC classes I, II, and IV require Zn^{2+} in the active site for enzymatic activity. HDAC class III enzymes do not contain zinc in the active site, but instead require NAD^{+} for their enzymatic activity (Witt *et al*., 2009).

Class I is comprised of HDACs 1, 2, 3, and 8 and are homologous to the yeast HDAC Rpd3 (Bolden *et al*., 2006). HDACs 1, 2, and 3 are localized in the nucleus and are ubiquitously expressed across various tissues. They are subunits of multi-protein complexes that are critical for

epigenetic landscaping and transcriptional repression. HDAC 8 shuttles between the nucleus and cytoplasm (Witt *et al*., 2009).

Class II HDACs share homology with yeast HDAC Hda1 and are subdivided into two groups: classes IIA and IIB. Class IIA consists of HDACs 4, 5, 7, and 9 which share an N-terminal domain that regulates shuttling between the nucleus and cytoplasm. Class IIB consists of HDACs 6 and 10 which are cytoplasmic. HDAC6 contains two tandem deacetylase domains, one of which is specific for α-tubulin thereby regulating cell adhesion and motility (Witt *et al*., 2009).

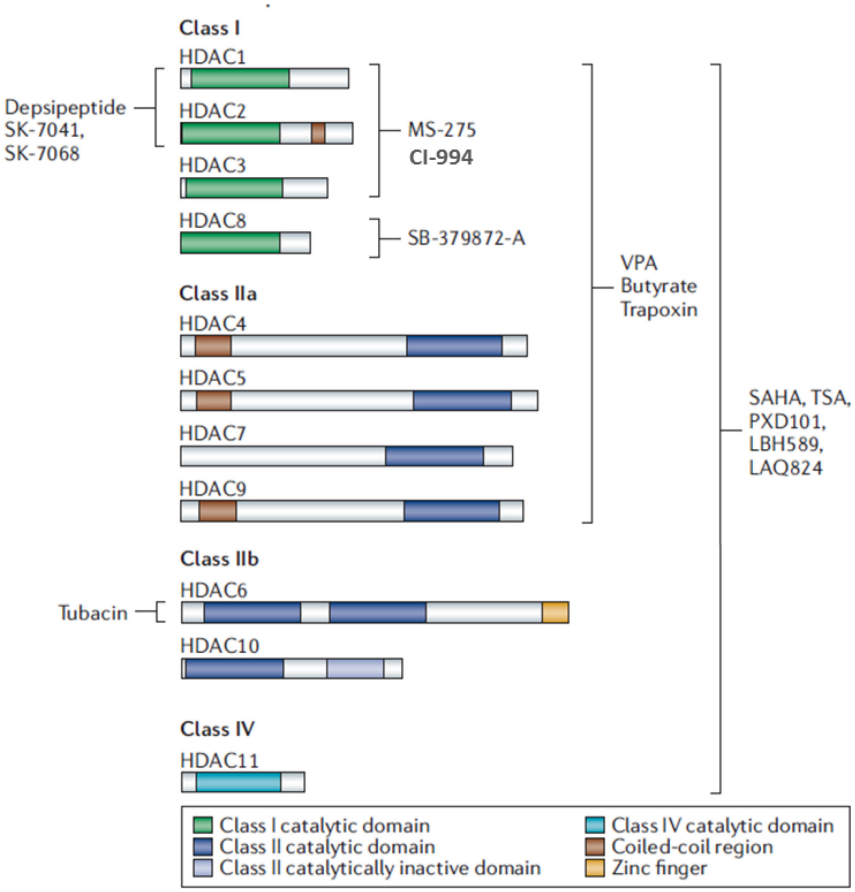

Figure 4. HDAC classes I, II, and IV and available inhibitors. Structural and functional domains are shown (Bolden *et al*., 2006).

Class III HDACs are named the sirtuins and share homology with the yeast HDAC Sir2. This class is comprised of SIRT 1, 2, 3, 4, 5, 6, and 7. Class IV consists solely of HDAC11. It does not have enough sequence identity to be placed in another class, but has conserved residues in its catalytic center that are shared by class I and class II HDACs (Bolden *et al*., 2006).

HDAC inhibitors can be grouped by structure into at least four different classes: hydroxamates, short-chain fatty acids, benzamides, and cyclic tetrapeptides (Bolden *et al*., 2006). Most hydroxamates are pan-inhibitors that inhibit class I and II HDACs by binding to the zinc atom in the catalytic site. They do not inhibit class III HDACs since they are zinc-independent (Witt *et al*., 2009). Examples include vorinostat (suberoylanilide hydroxamic acid or SAHA), trichostatin A (TSA), belinostat (PXD 101), panobinostat (LBH 589), and LAQ824 (Figure 4). Short-chain fatty acids such as valproic acid (VPA) and butyrate inhibit class I and IIa HDACs. The benzamides are selective inhibitors, which include MS-275 and CI-994 that inhibit HDACs 1, 2, and 3 (Beckers *et al*., 2007). Similarly, cyclic tetrapeptides such as depsipeptide selectively inhibit HDACs 1 and 2 (Ma *et al*., 2009).

1.5 Previous Research by the Rabson Laboratory

The Rabson Laboratory set out to determine if epigenetic therapy could be used to attenuate malignancies and convert them into manageable chronic diseases (personal communication). They chose to investigate this question using colorectal cancer cell lines since HDACs 1, 2, and 3 are commonly overexpressed in colon cancer (Bolden *et al*., 2006). Overexpression of HDACs in colon cancer correlates with tumor onset and progression (Bolden *et al*., 2006) and has been associated with reduced patient survival (Witt *et al*., 2009). Vorinostat was the HDAC inhibitor selected for testing since it had been demonstrated to induce growth arrest, differentiation, or

apoptosis in multiple cancer cell lines and several *in vivo* models of cancer (Kelly *et al*., 2003). Vorinostat was also in clinical trials and FDA approved for treatment of cutaneous T cell lymphoma (Dawson and Kouzarides, 2012).

With the model system selected, the Rabson lab began to test the hypothesis that long-term vorinostat treatment could inhibit the growth of colon cancer cells through epigenetic re-programming (personal communication). Work was performed using two human cell lines: SW480 from a primary colorectal adenocarcinoma and HCT-116 from a primary colorectal carcinoma. SW480 has mutant tumor suppressor gene *TP53*, mutant oncogene *KRAS*, and *MYC* amplification (Ahmed *et al.*, 2013; ATCC CCL-228™). HDACs 1 and 2 are highly expressed in SW480 (Bolden *et al*., 2006). HCT-116 has wild-type *TP53*, mutant *KRAS*, and *MYC* overexpression (Ahmed *et al.*; ATCC CCL-247™). A single colony subclone of SW480 cells, named S3, was selected and used for all experiments. One micromolar vorinostat-adapted cells, named SSH1, were generated by culturing S3 cells with 1 μM vorinostat for over 3 months. Three micromolar vorinostat-adapted cells, named SH80, were generated by initially culturing S3 cells with 1 μM vorinostat and increasing the dose in 1 μM increments every 2 – 3 weeks until 3 μM was reached. Other cells lines generated include: SH' cells which were SH80 cells culture without vorinostat for over 3 months and SR cells that are vorinostat resistant cells derived from being directly cultured with 3 μM vorinostat (Lin and Liu, Rabson Laboratory).

HCT-116 vorinostat-adapted cells, referred to as HCT adapted, were generated by culturing HCT-116 cells with 1 μM vorinostat for over 3 months (Lin, Rabson Laboratory).

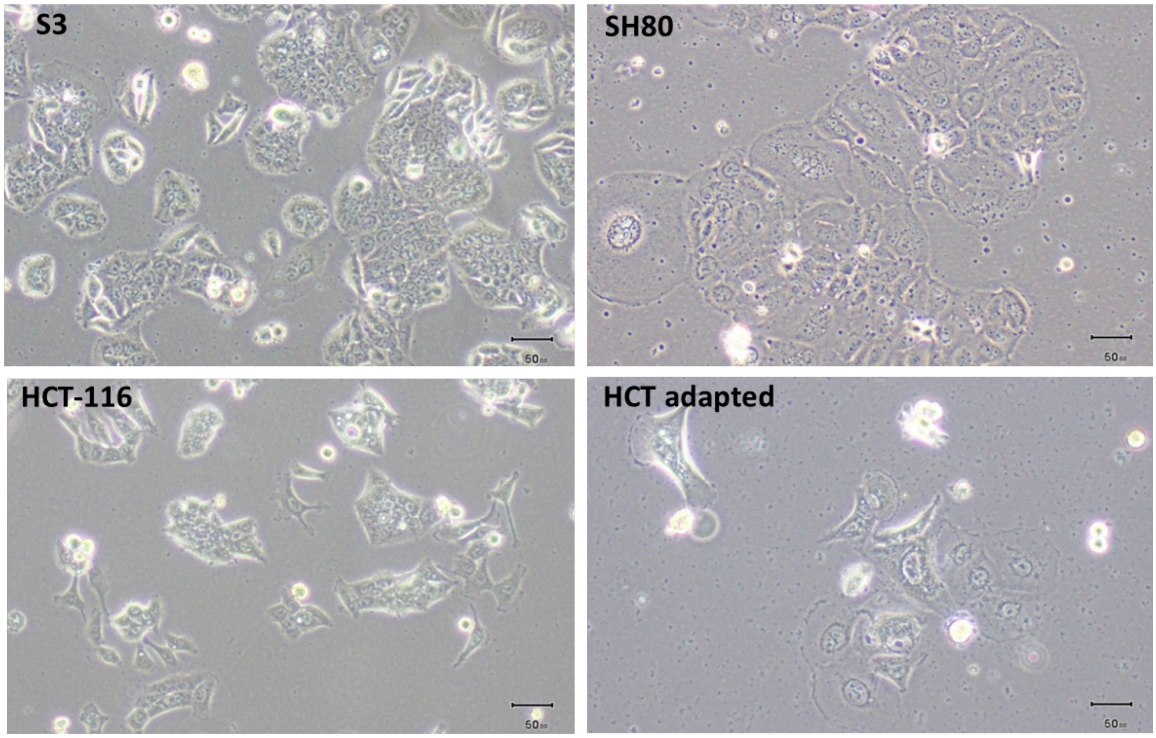

Figure 5. Morphology changes in vorinostat-adapted cells, SH80 and HCT adapted, compared to original carcinoma cells, S3 and HCT-116 (Lin, Rabson Laboratory).

SH80 and HCT adapted cells exhibited similar changes in morphology compared to S3 and HCT-116, respectively (Figure 5). Vorinostat-adapted cells had a marked increase in cell size. Some adapted cells were bi- or multi-nucleated, suggesting defective cytokinesis (Lin, Rabson Laboratory).

The cell proliferation rate was substantially reduced in SH80 compared to S3 with a 13-fold difference in the number of cells after 10 days (Figure 6A). The results were similar regardless of whether SH80 was cultured with or without 3 µM vorinostat, showing that the reduction in proliferation was due almost entirely to cellular changes from the adaptation. Cytotoxicity was observed for S3 cells treated directly with 3 µM vorinostat after 7 days in culture.

A similar reduction in the cell proliferation rate was observed for SH' compared to S3 with a 10-fold difference in the number of cells after 7 days, demonstrating that the 3 µM vorinostat-adapted cells retain the reduced proliferation phenotype even after long-term culture without the drug (Figure 6B). There was little difference in the proliferation rate between SH' cells cultured with and without 3 µM vorinostat, suggesting that the cells maintain the cellular state that allows them to tolerate the inhibitor.

Unlike SH80 and SH' cells, the proliferation rate of SR cells was only modestly slower compared to S3 cells with a 2-fold difference in the number of cells after 8 days, independent of whether or not the SR cells were cultured with 3 µM vorinostat (Figure 6C). The contrast between the proliferation rates of SH80 and SR relative to S3 indicated that the adaptation process was not merely a selection for cells resistant to vorinostat (Lin and Liu, Rabson Laboratory).

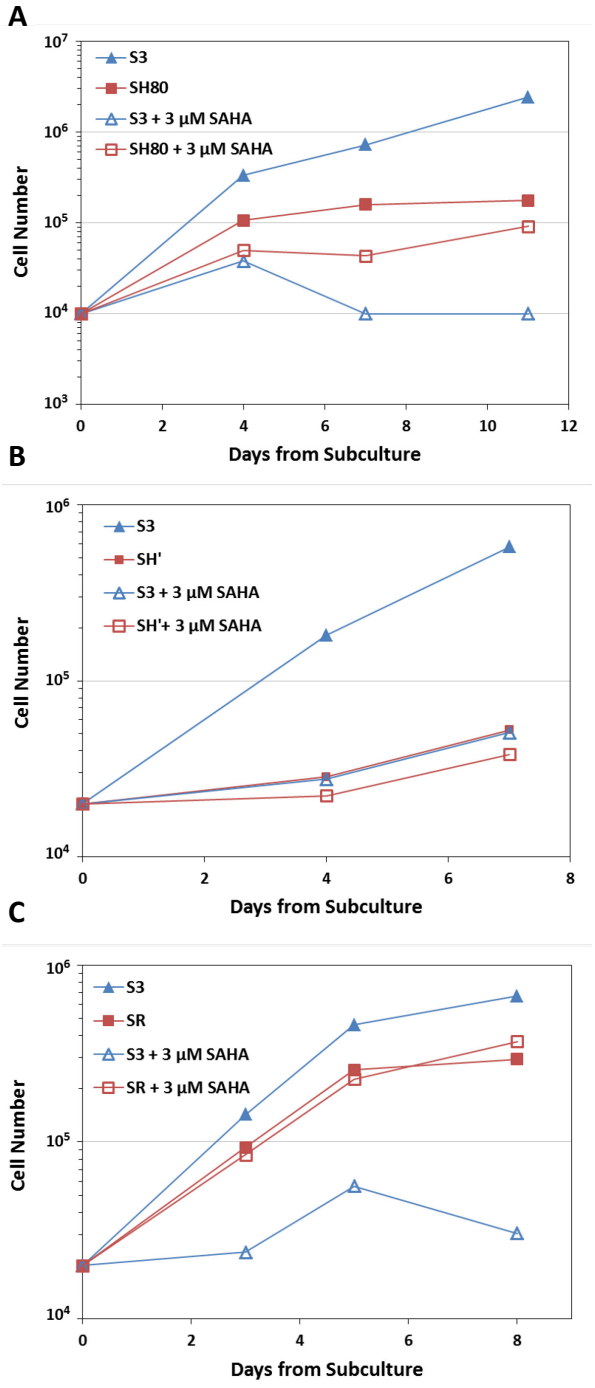

Figure 6. Cell proliferation assay for (A) S3 versus SH80 cells, (B) S3 versus SH' cells, and (C) S3 versus SR cells (Lin and Liu, Rabson Laboratory).

The cell proliferation rate was substantially reduced in HCT adapted cells compared to HCT-116 with a 10-fold difference in the number of cells after 11 days (Figure 7). Some cytotoxicity was observed for HCT-116 cells treated directly with 1 µM vorinostat after 4 and 6 days in culture. However, the proliferation rate of the acutely-treated cells rebounded after 11 days in culture, with double the number of cells compared to the HCT adapted cells. These results suggest there is a difference in phenotype between acutely treated HCT-116 cells and HCT adapted cells. Additional experiments are needed to establish that the HCT adapted cells are different from resistant cells selected by direct treatment with 1 µM vorinostat (Lin, Rabson Laboratory).

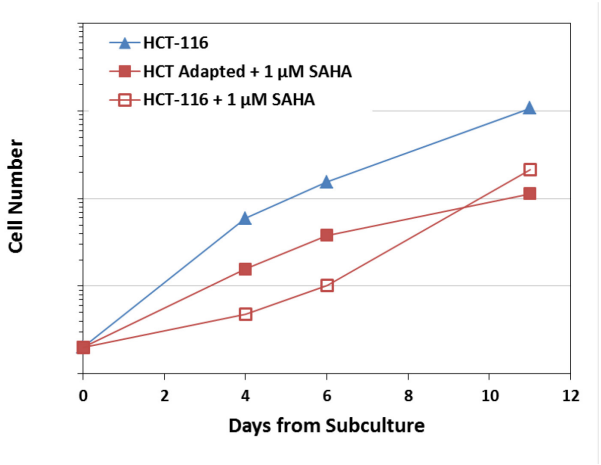

Figure 7. Cell proliferation assay for HCT-116 versus HCT adapted cells (Lin, Rabson Laboratory).

Both 3 µM vorinostat-adapted cell lines, SH80 and SH', showed a marked reduction in colony formation compared to S3 cells with only a few colonies formed per 1000 cells (Figure 8). The 1 µM vorinostat-adapted cell line SSH1 had a more than 3-fold reduction in colony formation compared to S3 cells. Interestingly, SR cells had an increase in colony formation compared to S3 cells.

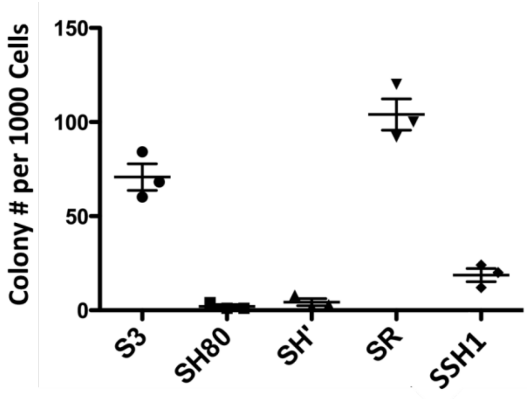

Figure 8. Colony formation assay for S3, SH80, SH', SR, and SSH1. Cells were cultured using methylcellulose-based medium (Lin and Liu, Rabson Laboratory).

These results reinforced the conclusions drawn from the cell proliferation assays in that the 3 µM vorinostat-adapted cells retained the reduced colony formation phenotype even after long-term culture without the inhibitor. Additionally, the striking difference in colony formation between SH80 and SR cells further supported the observation that the adapted cell lines are not a selection of vorinostat-resistant cells (Lin and Liu, Rabson Laboratory).

Similar results were seen with HCT adapted cells, which showed a marked reduction in colony formation compared to HCT-116 cells (Figure 9). An average of eight colonies formed per 1000 HCT adapted cells compared with an average of 190 colonies for HCT-116 cells (Lin, Rabson Laboratory).

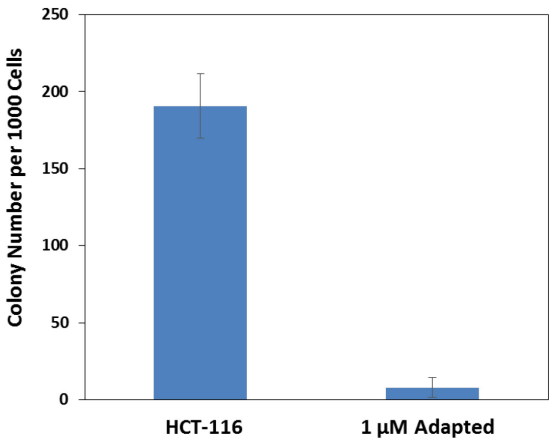

Figure 9. Colony formation assay for HCT-116 and HCT adapted. Cells were cultured using methylcellulose-based medium (Lin, Rabson Laboratory).

Tumor xenografts in athymic mice were used to evaluate the tumorigenicity of SH80 cells compared to S3 cells. For each cell type, ten mice were injected in the flanks subcutaneously with an equal number of cells. Tumor development was monitored over two months. No drug was administered to the mice. With S3 cells, 7 out of 10 mice formed tumors which increased in volumed over time (Table 2). In contrast, tumorigenicity was nearly eliminated in SH80 cells with only one small tumor forming over the 60 day observation period (Lin and Liu, Rabson Laboratory).

Table 2. Tumorigenicity of S3 and SH80 cells in athymic mice xenograft model (Lin and Liu, Rabson Laboratory).

Cell line	Tumor Incidence	Onset	Tumor Size (range in mm^3)		
			Day 20	Day 40	Day 60
S3	7/10	Day 18	20- 52	38 -145	85 -145
SH80	1/10	Day 35	0	0 - 17	0 - 21

The sum of these results demonstrated that long-term vorinostat treatment could inhibit the proliferation and tumorigenicity of colon cancer cells. In order to investigate some of the underlying mechanisms behind these changes, an Affymetrix U133A 2.0 Array was used to evaluate differences in gene expression between S3 and SH80 cells. Approximately 10% of genes in the array had more than a 2-fold difference in expression between the two cells lines, with 2/3 of those genes upregulated in SH80 (Lin, Rabson Laboratory). A bioinformatic analysis of the array data was performed using curated expression signatures from embryonic stem cells and breast cancer cells. An expression signature is defined as the consistent over- or under-expression of sets of genes that are associated with a biological state (Markert *et al*., 2011). The analysis found that vorinostat adaptation downregulated the stem cell gene expression signature (Markert, Cancer Institute of NJ), which was consistent with the more differentiated phenotype of the SH80 cells. Another notable result was that the gene expression signature of PRC2 targets was upregulated in SH80 cells, indicating a downregulation in the PcG system and/or an upregulation of TrxG system (Markert, Cancer Institute of NJ). This was consistent with the expectation that vorinostat-inhibition of HDACs 1 and 2 would prevent removal of the acetylation mark on H3K27, thus antagonizing PcG-mediated silencing at PRC2 target genes.

An alternate list of PRC2 target genes was acquired from results of a SUZ12 chromatin immunoprecipitation - human gene promoter array assay performed on SW480 cells (Squazzo *et al*., 2006). A subset of upregulated and downregulated genes were identified for further analysis from both lists of PRC2 target genes. Selected genes were associated with carcinogenesis, intestinal differentiation, and signal transduction pathways (Lin, Rabson Laboratory).

1.6 Thesis Research Goals

Given the global changes in gene expression in SH80 cells, the overarching goal of this thesis research was to narrow down the set of changes to what was necessary and sufficient to generate the non-malignant phenotype of SH80. Two approaches were used to work towards this goal.

The first approach was to identify changes in gene expression specific to the non-malignant phenotype for vorinostat-adapted cells. Based on the analysis of the gene expression microarray, we used H3K27 trimethylation and acetylation status to evaluate changes at PRC2 targets as a function of i) vorinostat concentration and ii) acute treatment versus adaptation with vorinostat.

The second approach was to determine if selective inhibition of HDACs 1, 2, and 3 in S3 is sufficient to generate the non-malignant phenotype. Since HDACs 1 and 2 have been shown to interact with PRC2 core components and are highly expressed in S3, we chose to adapt S3 cells to CI-994 and evaluate changes in proliferation, colony formation, and gene expression at PRC2 targets.

Chapter 2: Materials and Methods

2.1 Cell Culture

S3 (a single colony subclone of SW480 cells obtained from ATCC), SSH1, and SH80 cells were provided by Hsin-Ching Lin of the Rabson Laboratory. S3 cells were cultured in Dulbecco's Modified Eagle's Medium (DMEM; Sigma D5796) supplemented with 10% fetal bovine serum (Gemini Bio-Products, Benchmark FBS), 1% GlutaMAX (Gibco, #35050061), and 100 U/ml penicillin – 100 μg/ml streptomycin (Gibco, #15140122). SSH1 and SH80 cells were cultured in DMEM complete medium with 1 μM and 3 μM vorinostat, respectively. All cells were grown on various sized plates and incubated at 37°C with 5% CO_2. Cells in the log stage of growth were used for all experiments.

Cells were passaged by first aspirating the media from the plate. Cells were then rinsed with Dulbecco's Phosphate Buffered Saline (PBS; Sigma D8537) and the PBS was aspirated from the plate. Trypsin-EDTA (0.25%, Gibco) was added to the plate and incubated at 37°C for 3 - 4 minutes until the cells were no longer attached to the plate. DMEM complete medium was added to the plate at 5 times the amount of trypsin to neutralize the trypsin. Subcultures were generated by transferring a portion of the trypsinized cells to new plates.

2.2 Histone Deacetylase Inhibitors and Cytotoxicity

The histone deacetylase (HDAC) inhibitor vorinostat (suberoylanilide hydroxamic acid or SAHA) was obtained from Selleckchem. A 50 mM stock solution was prepared in dimethyl sulfoxide (DMSO; Sigma D2650). The 50 mM stock solution was diluted in culture medium to 10 μM for use in cell culture. HDAC inhibitor CI994 (tacedinaline) was obtained from Selleckchem. A 200

mM stock solution was prepared in DMSO, which was further diluted to 2 mM in DMSO. The 2 mM DMSO solution was diluted in culture medium to 50 µM for use in cell culture.

The MTT assay was used to measure the cytotoxicity of CI994 in S3 cells. Cells were seeded in a 96-well plate in 100 µl of medium with 2 x 10^3 cells per well. An additional 100 µl of media was added to each plate 20 – 24 hours after seeding, with media containing the appropriate concentration of CI994 for final concentrations ranging from 0 to 10 µM. Cells were grown in triplicate for each CI994 concentration for 6 days. The assay was performed by adding 20 µl of MTT solution (10 mg/ml MTT dissolved in PBS) to each well and incubated at 37°C for 3.5 hours. Media was then carefully aspirated from each well. One hundred fifty microliters of MTT solvent (4 mM HCl, 0.1% IGEPAL CA-630 in isopropanol) was added to each well. The plate was covered with foil and incubated for 15 min at room temperature on a platform shaker. The absorbance was read at 590 nm using a Perkin Elmer Victor X3, 2030 Multilabel Reader.

2.3 Counting Viable Cells

Viable cells were counted by trypsinizing cells as described above. A 10 µl aliquot of the suspended cells was transferred to a microfuge tube and 10 µl of 0.4% trypan blue (Sigma) was added to the tube and mixed. A 10 µl aliquot of the mixture was pipeted onto a hemacytometer. Cells were counted in the 4 corner squares of the hemacytometer and the average number of cells per square was determined. The number of cells per ml was calculated as follows:

$$\#\ \text{cells per ml} = (\text{average number of cells per square}) * (\text{dilution factor} \times 10^4).$$

When each corner of the hemacytometer had less than 20 cells, all 9 squares on the hemacytometer were counted to determine the average number of cells per square.

2.4 HDAC Inhibitor Adaptation

CI-994 adapted cells were generated by initially culturing S3 cells with 1 μM CI-994 and gradually increasing the dose every 3 – 4 weeks until concentrations of 9 μM and 12 μM were reached. The steps in CI-994 concentration were 1 to 5 μM in 1 μM increments, followed by increases to 7, 9, and finally 12 μM. Cells were passaged at least two times before proceeding with a dose increase.

2.5 Cell Proliferation Assay

Cells were seeded in a 12-well plate in 1 ml of media with 1 x 10^4 cells per well. An additional 1 ml of media was added to each plate 20 – 24 hours after seeding, with media for acute treatments containing the appropriate concentration of HDAC inhibitor. Cells were grown in triplicate for each HDAC inhibitor concentration. Wells were trypsinized and viable cells counted every 2 - 3 days after the start of treatment.

2.6 Clonogenic Assay

Two sets of 6-well plates were seeded for each HDAC inhibitor-adapted cell line. Plates were seeded with 100 and 250 cells per well in 3 ml of media, with each cell count seeded in triplicate. The assay was stopped after 8 and 10 days for S3, SSH1, and CI-994 adapted cell lines. The assay for SH80 was stopped after 8 and 14 days.

Cells were washed twice with ice-cold PBS then fixed with 100% ice-cold methanol for 10 minutes at 4°C. The methanol was removed from the plates and enough crystal violet solution (0.1% crystal violet in 10% ethanol) was added to cover the bottom of the wells. The plates

were incubated at room temperature for 10 minutes. The crystal violet solution was pipetted off and the plates were rinsed carefully with deionized water. Plates were allowed to air dry at room temperature. The number of colonies was counted for each cell line. The 250 cell seeding was used for counting when fewer than 50 colonies were formed. Otherwise, the 100 cell seeding was used for counting.

2.7 RNA Extraction and Reverse Transcription

RNA was purified from all cell lines using the Qiagen RNeasy Mini Kit. Cells were lysed directly on the tissue culture plate using 600 µl of Qiagen buffer RLT. Lysates were collected and stored at -80°C until ready for the RNA extraction. Lysates were homogenized using the Qiagen QIAshredder and the RNA extraction was performed according to the manufacturer's instructions, including the on-column DNase digestion. cDNA was prepared using SuperScript® VILO cDNA Synthesis Kit (Invitrogen) according to the manufacturer's instructions. One microgram of RNA was reverse-transcribed in a 10 µl reaction.

2.8 RNA qPCR Analysis

PowerUp SYBR Green Master Mix (Applied Biosystems) was used for all qPCR reactions. cDNA was diluted 1:10 and 1 µl of the diluted cDNA was used in each real-time quantitative PCR (qPCR) reaction. Real-time qPCR was performed on an Applied Biosystems QuantStudio 6 Flex instrument. The fold change in gene expression was determined using the comparative Ct method (ΔΔCt). TATA box binding protein (TBP) was used for the endogenous control. Acutely treated S3 cells and adapted cell lines were referenced to S3. A list of primer sequences is provided in Appendix A.1.

2.9 Antibodies

Chromatin immunoprecipitation (ChIP) antibodies included rabbit anti-trimethyl-H3K27 (#9733) obtained from Cell Signaling, which was used at a 1:100 dilution. Rabbit anti-H3 (ab1791), anti-acetyl-H3K27 (ab4729), and normal rabbit IgG (ab37415) were acquired from Abcam, with 5 µg of antibody used per IP.

2.10 Chromatin Immunoprecipitation of Histones

Cells were crosslinked for 5 min at room temperature by adding 1% formaldehyde (37% stock preserved with 15% methanol; EM Science FX0410-1) to the culture medium. Glycine was added to a final concentration of 0.125M and incubated for 5 min at room temperature to stop the cross-linking reaction. Cells were rinsed twice with cold PBS (Sigma D8537). Five milliliters of cold PBS with 5 mM EDTA was added to each 15 cm plate and incubated for 5 min at room temperature. Cells were then scraped down and transferred to a 50 ml conical. Each plate was rinsed with 4 ml of PBS and the remaining cells were transferred to the 50 ml conical. Cells were pelleted by centrifugation at 2000 rpm for 5 min at 4°C. The supernatant was poured off, cells were snap frozen using liquid nitrogen, and subsequently stored at -80°C until processing.

Cell membranes were lysed in 15 ml of PIPES lysis buffer (5 mM PIPES pH 8.0, 85 mM KCl, 0.5% IGEPAL CA-630, fresh 1 mM PMSF) for 25 min at 4°C on a rotator. Nuclei were pelleted by centrifugation at 2000 g for 5 min at 4°C. The supernatant was removed, nuclei were resuspended in 1.5 ml of SDS lysis buffer (0.5% SDS, 50 mM Tris pH 8.0, 10 mM EDTA, fresh 1 mM PMSF, fresh Roche complete protease inhibitor #11-836-170-001), transferred to a 5 ml round-bottom culture tube, and incubated for 30 min at 4°C on a platform shaker. Samples

were sonicated (Branson Digital Sonifier 450) 4 times at 45% amplitude for 10 sec, with 1 min rest on ice between sonications. Care was taken to avoid formation of bubbles/foam.

A small sample of DNA was purified from each lysate to check the sonication quality. Ten microliters of lysate was added to 50 µl of freshly prepared IP elution buffer (1% SDS, 0.1 M $NaHCO_3$). Cross-links were reversed by adding 2 µl of 5 M NaCl and boiling for 15 min. Samples were cooled to room temperature. One microliter of 50 µg/ml RNase A (Qiagen) was added and samples were incubated at 55°C for 5 min. DNA was purified using a PCR purification kit (Qiagen). Ten microliters of purified DNA and a 1 KB plus DNA ladder (Invitrogen) was run on a 1.2% agarose gel at 100 V for 30 min. Gels were imaged to visualize the distribution of DNA fragment sizes (target range of 500 – 1650 bp).

Each lysate was transferred to a microfuge tube and centrifuged at maximum speed for 15 min at 4°C. The supernatant was transferred to a fresh microfuge tube, centrifuged a second time, and transferred to a new microfuge tube. The DNA concentration of each lysate was measured on the NanoDrop 1000 Spectrophotometer. Lysates were stored at -80°C.

The appropriate volume of each lysate was transferred to a 15 ml conical tube so that each immunoprecipitation (IP) would contain 125 µg of DNA. Lysates were diluted 1:5 with IP dilution buffer (20 mM Tris pH 8.1, 150 mM NaCl, 2m M EDTA, 1% Triton X-100, fresh 1 mM PMSF) with a final volume of 1.2 ml per IP. Diluted samples were pre-cleared with 30 µl of protein A agarose beads (EMD Millipore 16-157) per IP for 2 hours at 4°C on a rotator. Pre-cleared samples were centrifuged at 2500 g for 5 min at 4°C. The supernatant was collected and divided into 1.2 ml aliquots in microfuge tubes for each IP, with 1% of the supernatant reserved

for the input. Antibodies were added to each IP sample and incubated overnight at 4°C on a rotator. Inputs were stored at -20°C.

Immune complexes were precipitated by adding 40 µl of protein A agarose beads to each IP and incubating for 1 hr at 4°C on a rotator. Samples were centrifuged at 2000 rpm for 1 min at 4°C and the supernatant discarded. Protein A agarose beads were washed with 1 ml of wash buffer for 5 min at 4°C on the rotator in the following order: two low salt washes (20 mM Tris pH 8.1, 150 mM NaCl, 2 mM EDTA, 1% Triton X-100, 0.1% SDS), two high salt washes (20 mM Tris pH 8.1, 500 mM NaCl, 2 mM EDTA, 1% Triton X-100, 0.1% SDS), one lithium chloride wash (10 mM Tris, 250 mM LiCl, 1 mM EDTA, 1% sodium deoxycholate, 1% IGEPAL CA-630), and two TE washes (10 mM Tris pH 8.1, 1 mM EDTA). Complexes were eluted twice by adding 200 µl of freshly prepared IP elution buffer (1% SDS, 0.1 M $NaHCO_3$), vortexing for 10 sec, incubating at room temperature for 15 min on a rotator, centrifuging at 2000 rpm for 1 min, and transferring the supernatant. Enough IP elution buffer was added to each saved input for a total volume of 200 µl. Cross-links were reversed by adding NaCl to a final concentration of 200 mM per sample and incubating overnight at 65°C. Proteins were broken down by adding 28 µl of proteinase K solution (600 mM Tris pH 6.5, 140 mM EDTA, 1.4 mg/ml proteinase K) per eluate (14 µl per input) and incubating for 1 hr at 55°C. Samples were purified using the Qiagen QIAquick Spin PCR Purification Kit. Genomic DNA was eluted once in 100 µl of EB. Each real-time qPCR reaction used 1.5 µl of genomic DNA.

2.11 ChIP qPCR Analysis

PowerUp SYBR Green Master Mix (Applied Biosystems) was used for all qPCR reactions. Real-time qPCR was performed on an Applied Biosystems QuantStudio 6 Flex instrument. All ChIP

primer sets amplified the gene promoter region. A list of primer sequences is provided in Appendix A.2. ChIP-qPCR data was analyzed for each antibody using the percent input method. First, the input was adjusted from 1% to 100% by subtracting 6.644 from the input Ct value. The percent input was then calculated as follows:

Percent input = 100*2^(Adjusted input Ct – antibody Ct).

The percent input of H3K27 trimethylation and acetylation was ratioed to the percent input of total H3.

Multiple comparison testing was performed using the Holm-Šidák method to determine statistical significance between treatments. A Family-Wise Error Rate (FWER) of 0.05 was used for all tests. All calculations were performed using GraphPad Prism 6.07 for Windows, GraphPad Software, La Jolla California USA, www.graphpad.com.

Chapter 3: Results

3.1 Changes in mRNA Expression and H3K27 Modifications Due to Acute Treatment and Adaptation with Vorinostat

In order to investigate the effects of vorinostat on S3 cells as a function of concentration and treatment type, S3 cells were treated directly with 1 µM and 3 µM vorinostat for 96 hours and harvested. In addition, vorinostat-adapted cell lines SSH1 and SH80 were grown and harvested. RNA extractions were performed for the evaluation of changes in mRNA expression using RT-qPCR. ChIP assays were used to assess changes in H3K27 trimethylation and acetylation at the promoter of select PRC2 target genes that showed altered expression in SH80 (per the gene expression microarray).

3.1.1 Effect of Vorinostat Concentration and Adaptation on the Relative Expression of PRC2 Target Genes

Two PRC2 target genes, *TSPAN8* and *STMN2*, showed substantial concentration- and adaptation-dependent increases in gene expression (Table 3). *TSPAN8* had a striking upregulation in gene expression only in SH80 cells, with comparatively minor changes in expression in acutely treated cells. In contrast, *STMN2* had large stepwise increases as a function of concentration and adaptation with the highest levels of expression occurring in SH80 cells.

Four PRC2 target genes (*DACH1, GAL, WT1, EDN3*) showed changes in gene expression as a function of either vorinostat concentration or adaptation. *DACH1* had a modest upregulation of expression in 3 µM acutely-treated cells and SH80. Expression of both *GAL* and *WT1* was downregulated in a concentration-dependent manner, independent of treatment type. In

contrast, downregulation of *EDN3* was substantially higher in the adapted cell lines compared to the 96 hour treatments.

Table 3. Fold change in expression of select genes for S3 cells treated acutely for 96 hours with 1 μM and 3 μM vorinostat, and vorinostat-adapted cell lines SSH1 and SH80. Differences are expressed relative to S3, with positive values indicating a fold increase and negative values indicating a fold decrease. Acute treatment and adapted columns were determined by RT-qPCR. The last column shows the fold difference in gene expression in SH80 relative to S3 from the Affymetrix U133A 2.0 Array.

PRC2 Target Genes

	Fold Change Relative to S3				
	Acute Treatment		Adapted		Microarray
Genes	1 μM – 96 h	3 μM – 96 h	SSH1	SH80	SH80
TSPAN8	3.0	7.7	-1.5	95.6	112.4
CYP24A1	3.2	7.3	37.1	9.1	31.2
RNF128	13.3	16.2	12.3	16.1	18.3
STMN2	>6.6	>61.4	>38.4	>1,271	18.2
DACH1	2.7	3.7	1.2	7.0	9.4
GATA6	9.7	11.1	8.4	6.4	5.5
GAL	-4.2	-10.4	-4.9	-25.8	-24.5
EDN3	-51.2	-24.0	> -2,018	> -2,149	-21.6
WT1	-2.0	-7.9	-2.7	-10.8	-9.9

Non-PRC2 Target Genes

	Fold Change Relative to S3				
	Acute Treatment		Adapted		Microarray
Genes	1 μM – 96 h	3 μM – 96 h	SSH1	SH80	SH80
SNAI2	3.6	9.0	1.4	5.6	6.7
DKK4	-1.3	-2.1	-4.5	-49.6	-470
EZH2	-1.1	-1.4	-2.2	-2.0	1.0
SUZ12	-1.4	-1.7	-1.9	-2.9	-1.6

Expression of the PRC2 target genes *RNF128* and *GATA6* were upregulated independent of vorinostat concentration and adaptation. *CYP24A1* showed inconsistent changes across the various treatments. Core components of the PRC2 complex, *EZH2* and *SUZ12*, showed little to no change in gene expression regardless of the concentration or treatment type.

Two non-PRC2 targets (*SNAI2, DKK4*) were tested for concentration- and adaptation-dependent changes in gene expression. *SNAI2* showed a modest upregulation of expression in 3 μM acutely-treated cells and SH80 while *DKK4* displayed a substantial downregulation of expression only in SH80.

3.1.2 Effect of Vorinostat Concentration and Adaptation on the Modification of H3K27 at PRC2 Target Gene Promoters

Three upregulated PRC2 target genes (*CYP24A1, DACH1, GATA6*) showed large increases of H3K27ac with a concomitant decrease in H3K27me3 in vorinostat acutely-treated and adapted cells at both concentrations. *CYP24A1* had a loss of trimethylation that was statistically significant (FWER = 0.05) for all vorinostat treatments compared to S3, except for SSH1 (Figure 10A). The gain of acetylation was significant for all treatments compared to S3. Increases in acetylation showed an adaptation-dependent response for both 1 μM and 3 μM concentrations. For *DACH1* and *GATA6*, there was a significant decrease in trimethylation and increase in acetylation for all treatments compared to S3 (Figures 10B and 10C). A concentration and adaptation dependent increase in acetylation was observed for SH80 compared to SSH1 and 3 μM acute cells, respectively.

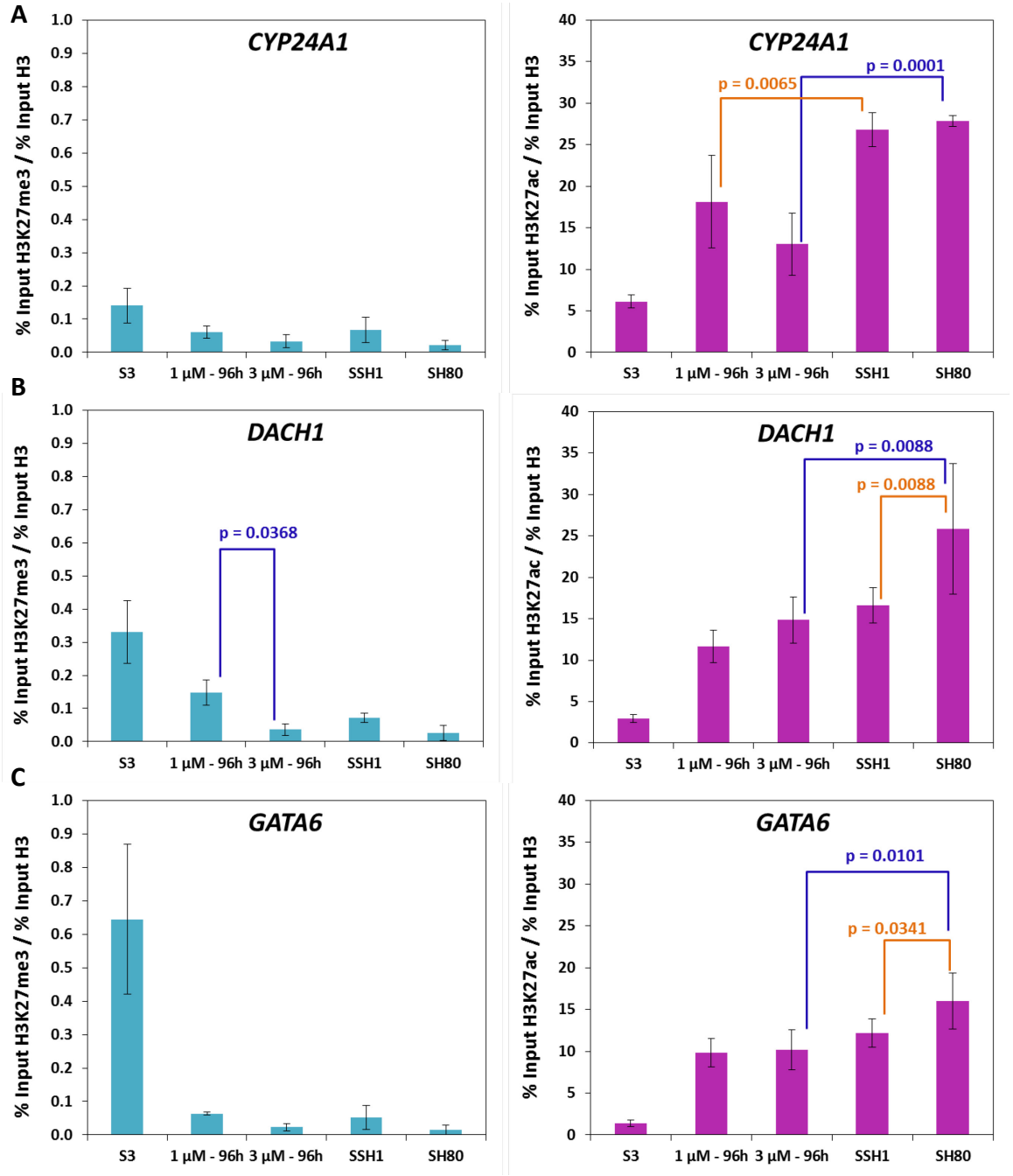

Figure 10. Upregulated PRC2 targets that switch at H3K27 from trimethylation to acetylation in vorinostat acutely-treated and adapted cells. Columns are the mean of 3 biological replicates with error bars representing ±1 SD. Multiplicity adjusted p-values for statistically significant results (FWER = 0.05) between acutely-treated and adapted cells are shown on the graphs.

Three upregulated PRC2 target genes (*TSPAN8, RNF128, STMN2*) showed decreases in H3K27me3 and modest increases in H3K27ac as a function of vorinostat concentration and/or adaptation. For *TSPAN8*, a significant reduction of trimethylation occurred for all vorinostat treatments compared to S3 (Figure 11A). Increased acetylation was only significant for 3 μM acute and SH80 cells relative to S3. A significant concentration-dependent effect was observed between SSH1 and SH80 for both loss of trimethylation and gain of acetylation. Additionally, there was a significant concentration-dependent increase in acetylation from 1 μM to 3 μM acutely treated S3 cells. For *RNF128*, decreases in H3K27me3 were adaptation-dependent, with significant decreases in SSH1 and SH80 compared to 1 μM and 3 μM acutely-treated cells, respectively (Figure 11B). Changes in H3K27ac were statistically significant for all vorinostat treatments compared to S3, except for SH80. A significant increase in H3K27ac occurred in 3 μM acutely-treated cells compared to 1 μM acutely-treated cells. Interestingly, a significant decrease in H3K27ac was observed in SH80 cells relative to 3 μM acutely-treated cells. At *STMN2*, a significant reduction of trimethylation occurred for all vorinostat treatments compared to S3 (Figure 11C). A significant concentration-dependent effect was observed between SSH1 and SH80 for both loss of trimethylation and gain of acetylation. Additionally, a concentration-dependent increase in acetylation occurred in 3 μM acutely-treated cells compared to 1 μM acutely-treated cells. *STMN2* also showed an adaptation-dependent decrease in trimethylation and increase in acetylation in SH80 compared to 3 μM acutely-treated cells.

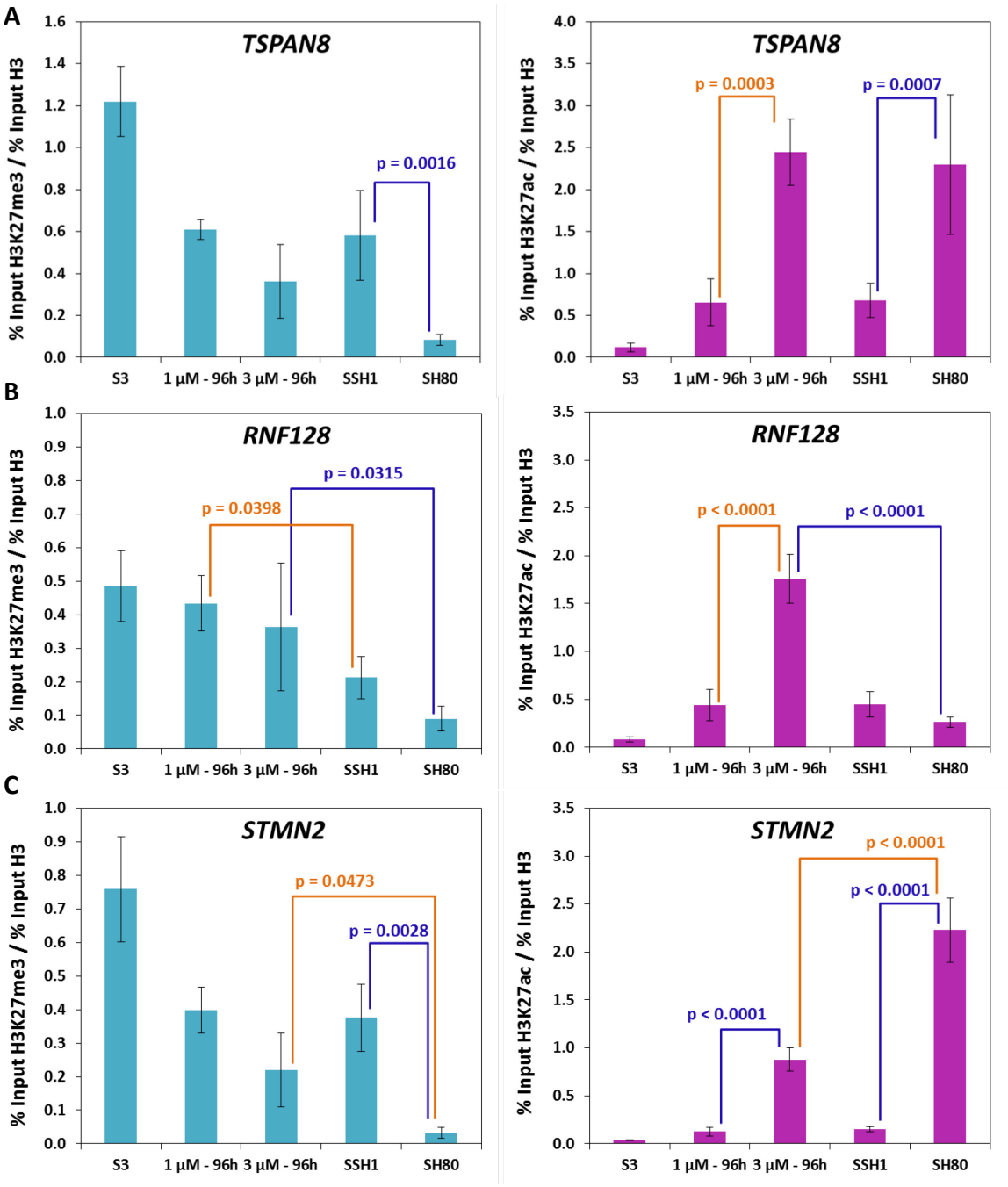

Figure 11. Upregulated PRC2 targets that switch at H3K27 from trimethylation to acetylation as a function of vorinostat concentration and/or adaptation. Columns are the mean of 3 biological replicates with error bars representing ±1 SD. Multiplicity adjusted p-values for statistically significant results (FWER = 0.05) between acutely-treated and adapted cells are shown on the graphs.

Two downregulated PRC2 target genes (*EDN3, GAL*) showed adaptation-dependent increases in H3K27me3. *EDN3* had a significant increase in trimethylation for SSH1 and SH80 compared to 1 µM and 3 µM acutely-treated cells, respectively (Figure 12A). Similarly, a significant decrease in acetylation was observed for SSH1 and SH80 compared to 1 µM and 3 µM acutely-treated cells, respectively. The reduction of H3K27ac was significant for all treatments compared to S3. For GAL, a significant increase in trimethylation occurred for SSH1 and SH80 compared to S3 (Figure 12B).

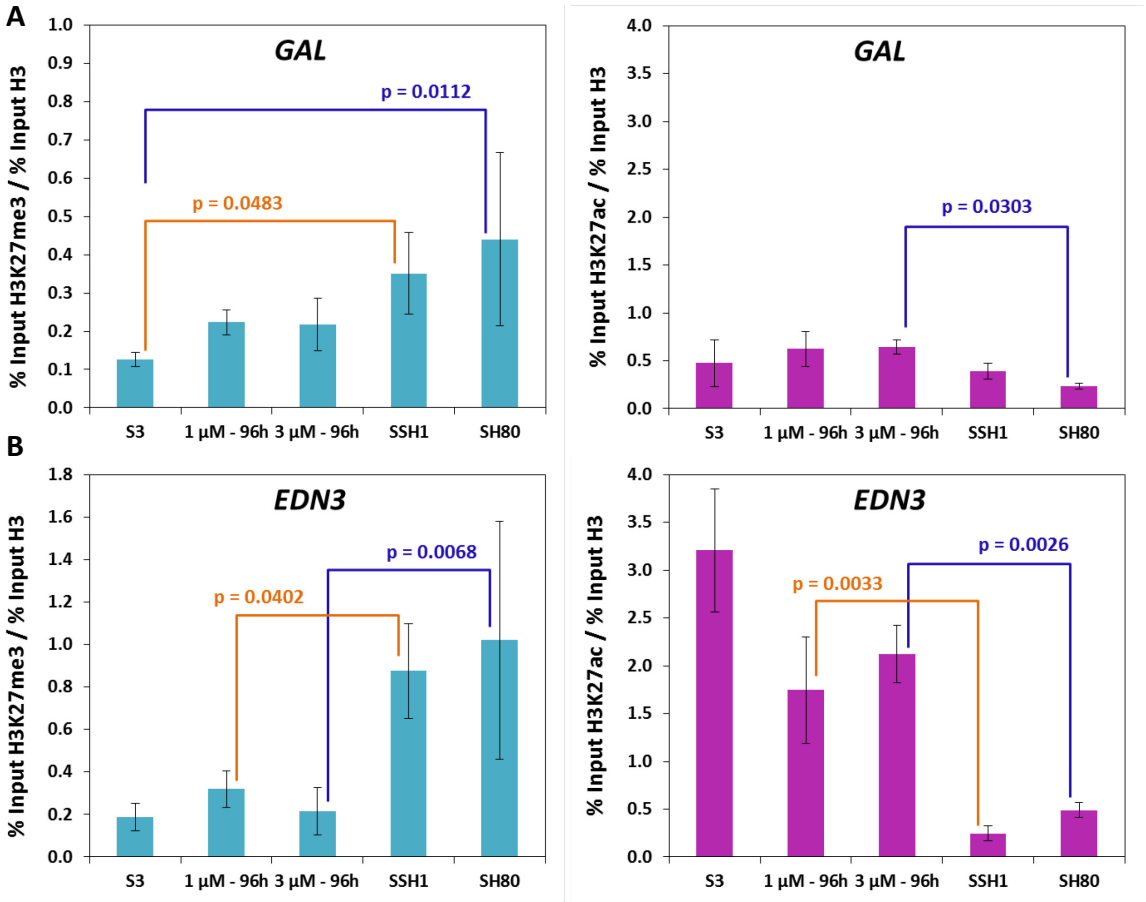

Figure 12. Downregulated PRC2 targets that switch at H3K27 from acetylation to trimethylation dependent on vorinostat adaptation. Columns are the mean of 3 biological replicates with error bars representing ±1 SD. Multiplicity adjusted p-values for statistically significant results (FWER = 0.05) between acutely-treated and adapted cells are shown on the graphs.

The downregulated PRC2 target *WT1* showed no significant changes in H3K27 trimethylation and acetylation between any of the cell lines (Figure 13). The non-PRC2 target *SNAI2* had negligible H3K27me3 across all cell lines (Figure 14). *SNAI2* H3K27ac was substantial in S3 cells and showed a significant increase for all treatments compared to S3, except 3 µM acutely-treated cells.

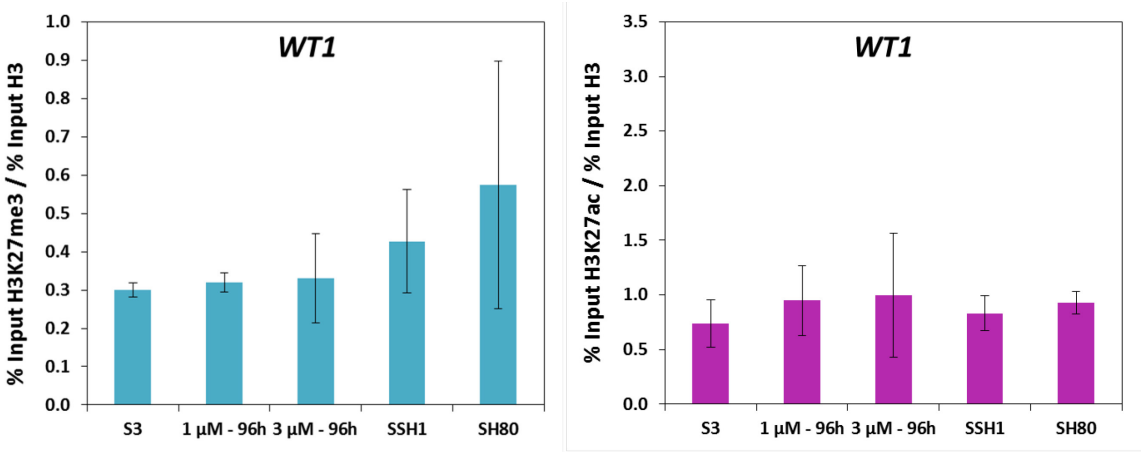

Figure 13. Downregulated PRC2 target with no statistically significant changes in H3K27 trimethylation and acetylation between any of the cell lines. Columns are the mean of 3 biological replicates with error bars representing ±1 SD.

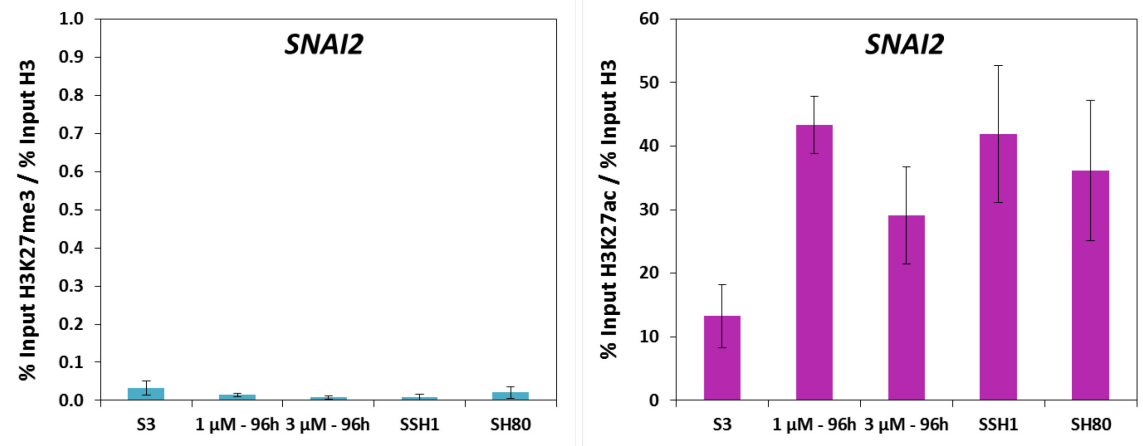

Figure 14. Non-PRC2 target with significant increases in H3K27 acetylation in 1 µM acutely-treated cells, SSH1, and SH80. Columns are the mean of 3 biological replicates with error bars representing ±1 SD.

3.2 Changes in Proliferation, Colony Formation, and mRNA Expression Due to CI-994 Adaptation

In order to determine if selective inhibition of HDACs 1, 2, and 3 is sufficient to generate a non-malignant phenotype, S3 cells were adapted to 9 and 12 µM CI-994. The adapted cells were characterized by performing proliferation and clonogenic assays. RT-qPCR was used to evaluate changes in mRNA expression at the same genes selected for the vorinostat studies.

3.2.1 Concentration Dependent Cytotoxicity of CI-994 in S3 cells

In order to determine the working concentration range of CI-994 in S3 cells, the cytotoxicity of CI-994 was measured using the MTT assay. CI-994 was cytotoxic to S3 cells at micro-molar concentrations, with an LD50 of approximately 3 µM and 80% cell death at 10 µM (Figure 13). Adaptation of S3 cells to CI-994 was started at 1 µM, which caused 27% cell death.

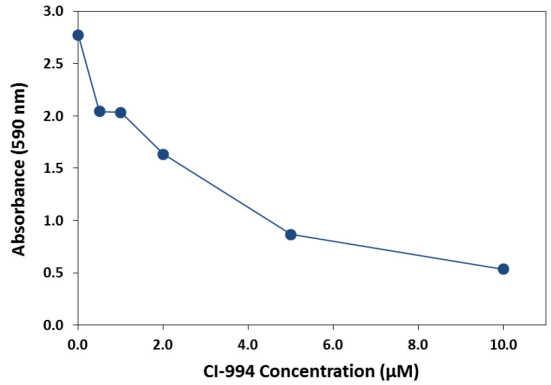

Figure 15. Cytotoxicity of CI-994 in S3 cells. Each data point represents the average of 3 plated replicates from one biological sample.

3.2.2 S3 Cells Adapted to CI-994 Have a Slower Proliferation Rate

S3 cells were adapted to 9 and 12 µM CI-994 over a 5 and 6 month period, respectively. A cell proliferation assay was performed to characterize the proliferation rates of the adapted cell lines. The cell proliferation rate was substantially reduced in 9 and 12 µM CI-994 adapted cells compared to S3 cells, with a 12-fold and 22-fold difference in the number of cells after 12 days, respectively (Figure 14). S3 cells treated acutely with 9 µM CI-994 showed a significant

inhibition of cell proliferation compared to S3 and CI-994 adapted cells, with almost no change in the cell number from days 7 through 12. Marked cytotoxicity was observed for S3 cells treated directly with 12 µM CI-994 after 7 days in culture.

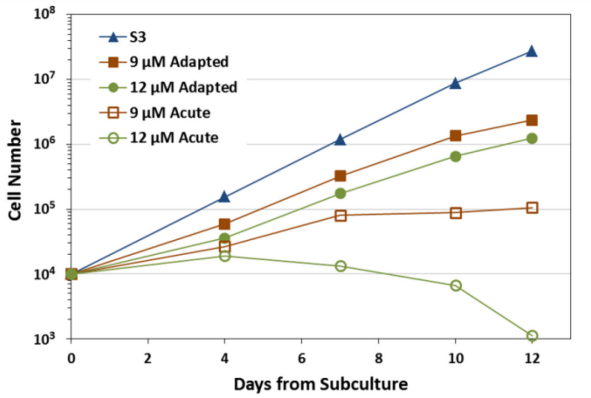

Figure 16. Cell proliferation rate of 9 and 12 µM CI-994 adapted cells. Each data point represents the average of 3 plated replicates from one biological sample.

3.2.3 Cells Adapted to 9 and 12 µM CI-994 Show Reduced Colony Formation

A clonogenic assay was performed to determine the ability of single cells to form colonies. Compared to S3 cells, 9 µM CI-994 adapted cells had a 33% reduction in colony formation (Figure 15). A marked reduction in colony formation was seen with 12 µM CI-994 adapted cells, which had a 63% reduction in colony formation compared to S3 cells. The largest reduction in colony formation was observed with SSH1 and SH80 cells, which both showed a 76% reduction in colony formation versus S3 cells. Some cell migration was observed for S3 and SSH1 cells which may have lowered the number of colonies counted.

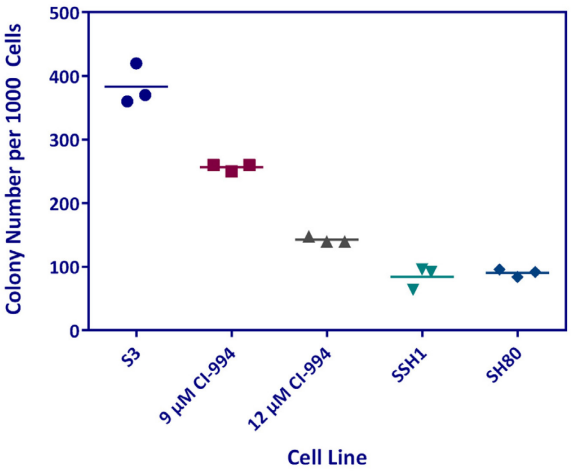

Figure 17. Clonogenic assay of S3, 9 and 12 µM CI-994 adapted cells, SSH1, and SH80 cells. Horizontal bars represent the average of 3 plated replicates from one biological sample.

3.2.4 Altered Expression of PRC2 Target Genes in CI-994 Adapted Cells Relative to S3

PRC2 target genes with upregulated expression in SH80 showed a similar increase in expression in CI-994 adapted cells relative to S3 cells (Table 4). Expression of *GAL* and *EDN3* was downregulated comparably in CI-994 adapted cells versus SH80 cells. In contrast, *WT1* was minimally downregulated in CI-994 adapted cells. Core components of the PRC2 complex, *EZH2* and *SUZ12*, showed no change in gene expression in CI-994 adapted cells. In contrast to SH80 cells, *SNAI2* showed no change in expression and *DKK4* showed only a modest decrease in expression in CI-994 adapted cells. No major differences in gene expression was observed between 9 μM and 12 μM CI-994 adapted cells at the selected PRC2 and non-PRC2 target genes.

Table 4. Fold change in expression of select genes for 9 μM and 12 μM CI-994 adapted cells. Differences are expressed relative to S3 cells, with positive values indicating a fold increase and negative values indicating a fold decrease. Expression levels were determined by RT-qPCR.

PRC2 Target Genes

	Fold Change Relative to S3	
	CI-994 Adapted	
Genes	9 μM	12 μM
TSPAN8	28.9	32.0
CYP24A1	53.2	53.5
RNF128	18.8	14.3
STMN2	235	428
DACH1	6.2	7.7
GATA6	12.5	15.8
GAL	-11.0	-8.8
EDN3	-1,462	> -363
WT1	-2.2	-2.5

Non-PRC2 Target Genes

	Fold Change Relative to S3	
	CI-994 Adapted	
Genes	9 μM	12 μM
SNAI2	1.6	1.1
DKK4	-5.5	-7.6
EZH2	-1.6	-1.3
SUZ12	-1.8	-1.5

Chapter 4: Discussion

4.1 Genes of Interest Identified in Vorinostat Treated Cells

While PRC2 target genes showed altered expression with vorinostat treatment, the response as a function of vorinostat concentration and adaptation was varied. All combinations of possible responses were observed: altered expression independent of concentration and adaptation, altered expression as a function of concentration, altered expression as a function of adaptation, and altered expression dependent on concentration and adaptation. *CYP24A1*, *DACH1*, *GATA6*, and *RNF128* displayed moderate increases in RNA levels that were relatively consistent across all of the treatments, with the exception of *CYP24A1* in SSH1. *GAL* and *WT1* had moderate decreases in RNA levels in 3 μM acutely treated and adapted cells. Most notably, *TSPAN8* and *STMN2* showed unusually large increases in expression in SH80, while expression of *EDN3* was substantially decreased in SSH1 and SH80. PRC2 targets upregulated with vorinostat treatment had similar levels of basal expression in S3, except *STMN2* which was at least 30 times lower. Thus, the large increase in expression of *STMN2* with vorinostat treatment, and particularly in SH80, was likely due to the gene switching from transcriptional silence to activation. Conversely, the extremely large decrease in expression of *EDN3* in SSH1 and SH80 was likely due to the gene becoming transcriptionally silent with vorinostat adaptation, independent of concentration. PRC2 targets downregulated with vorinostat treatment had higher levels of basal expression compared to the upregulated PRC2 targets investigated. Expression of *EZH2* and *SUZ12* was relatively unchanged by vorinostat treatment, indicating that the changes observed at PRC2 target genes are not due to changes in RNA levels of the core components of the PRC2 complex. A western blot is needed to determine if there are any changes in *EZH2* or *SUZ12* protein levels and might also reveal changes in protein mobility of these PRC2 complex components that might reflect altered post-translational modifications.

Similar to the observed changes in mRNA levels, PRC2 target genes showed changes in H3K27 trimethylation and acetylation with vorinostat treatment, but the response as a function of vorinostat concentration and adaptation was again varied. All combinations of responses to concentration and adaption were observed. S3 cells had modest levels of H3K27ac for *CYP24A1*, *DACH1*, and *GATA6*. These loci had substantial increases in acetylation with an almost complete loss of trimethylation for all vorinostat treatments. Compared to the relatively consistent mRNA levels across vorinostat treatments, these results suggest that there is a saturation point for acetylation of H3K27 above which the level of transcription remains constant.

The three genes with the most striking changes in mRNA expression as a function of vorinostat concentration and/or adaptation showed equally interesting changes in H3K27 modifications. *TSPAN8* switched from having high levels of trimethylation and almost no acetylation at H3K27 in S3 cells to having moderate levels of acetylation and almost no trimethylation in SH80 cells, which was

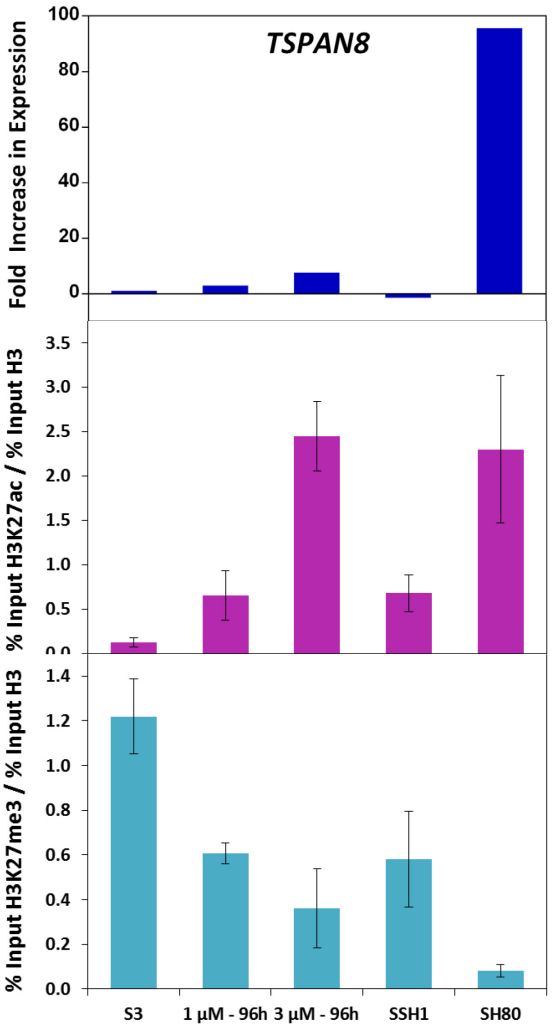

Figure 18. Comparison of *TSPAN8* mRNA expression and modification of H3K27 for vorinostat-treated cells. The top graph shows the fold increase in mRNA expression. The middle and bottom graphs show H3K27 ac and me3 levels, respectively.

consistent with the large increase in mRNA levels observed in SH80 (Figure 16). While the 3 µM acutely treated cells showed a comparable increase in H3K27ac compared to SH80, they did not have a complete loss of H3K27me3. This may be reflected by the relatively small increase in *TSPAN8* RNA expression in 3 µM acutely treated cells.

Similar to *TSPAN8*, *STMN2* switched from having high levels of trimethylation and almost no acetylation at H3K27 in S3 cells to having moderate levels of acetylation and almost no trimethylation in SH80 cells, with a correspondingly large increase in mRNA expression in SH80 (Figure 17). Although dwarfed by the extreme change in gene expression in SH80, substantial increases in mRNA levels were observed for 3 µM acutely-treated cells and SSH1. The 3 µM acutely-treated cells showed a modest increase in H3K27ac, but only a partial loss of trimethylation. The results of both TSPAN8 and STMN2 suggest that loss of H3K27me3 may have a stronger influence on gene expression than increased H3K27ac at certain loci. mRNA levels in SSH1 were somewhat inconsistent with the changes in H3K27 modifications.

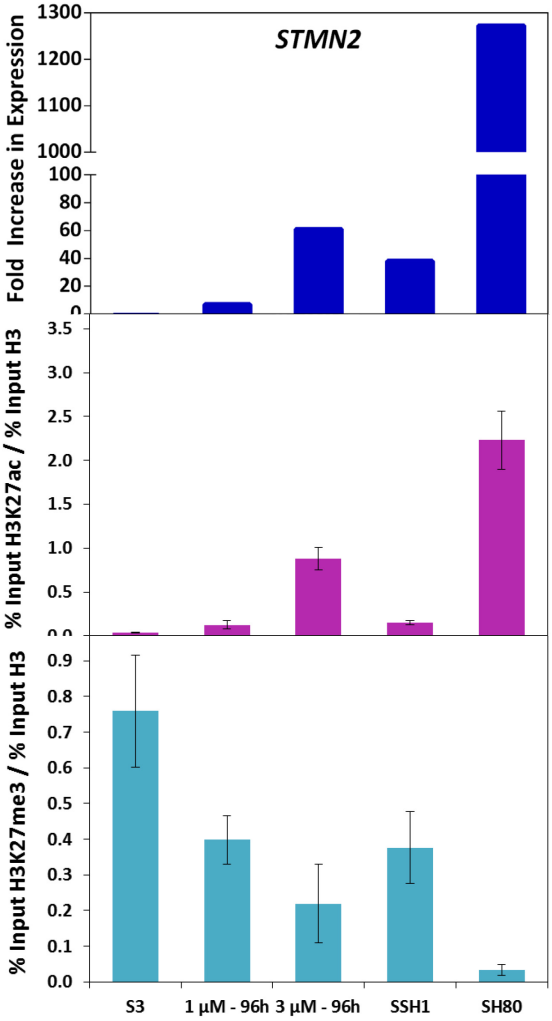

Figure 19. Comparison of *STMN2* mRNA expression and modification of H3K27 for vorinostat-treated cells. The top graph shows the fold increase in mRNA expression. The middle and bottom graphs show H3K27 ac and me3 levels, respectively.

In contrast to *TSPAN* and *STMN2*, *EDN3* switched from having low levels of trimethylation and moderate levels of acetylation at H3K27 in S3 cells to having low levels of acetylation and high levels of trimethylation in SSH1 and SH80 cells. Large decreases in mRNA expression were observed in SSH1 and SH80, with the gene becoming transcriptionally silent (Figure 18). Both 1 µM and 3 µM acutely-treated cells showed a substantial reduction in mRNA levels which corresponded with a reduction in H3K27ac.

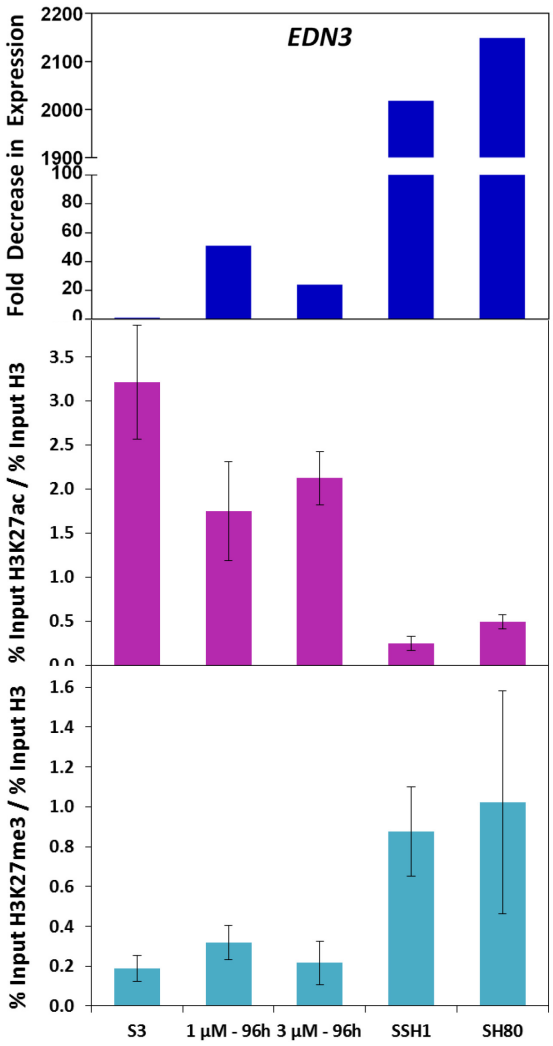

Figure 20. Comparison of *EDN3* mRNA expression and modification of H3K27 for vorinostat-treated cells. The top graph shows the fold decrease in mRNA expression. The middle and bottom graphs show H3K27 ac and me3 levels, respectively.

Given the dependence on concentration and/or adaptation and the correlation between mRNA expression and H3K27 modifications, *TSPAN8*, *STMN2*, and *EDN3* are examples of genes whose changes in mRNA expression and histone modifications may be associated with the oncogenic potential of this set of colon cancer cells and, therefore, should be investigated further to determine their importance in generating the non-malignant phenotype.

Gene expression levels and H3K27 modifications were inconsistent for *RNF128* and *WT1*. *RNF128* showed a consistent increase in expression across all vorinostat treatments. However, H3K27me3 decreased only in SSH1 and SH80 while H3K27ac increased modestly in both acute treatments and SSH1. *WT1* had reduced expression in 3 μM acutely-treated cells and SH80. However, there were no significant changes in H3K27 trimethylation or acetylation across all cell lines. For GAL, there were high standard deviations for H3K27me3 in several treatments, making comparisons to this data questionable.

Inconsistencies between gene expression and H3K27 modifications may be due to several factors. The work to date does not consider the influence of other histone modifications on transcription. A better characterization of the epigenetic landscape is required to fully understand the changes in gene expression due to vorinostat treatment. For example, it would be useful to look for changes in the TrxG activating marks H3K4me3 and H3K36me2 to get a better picture of the antagonist effects between the PcG and TrxG systems at each locus. Another factor that was not covered by this research was changes in PRC1 activity or expression of PRC1 core components. While the PRC2 complex establishes H3K27me3, the PRC1 complex binds H3K27me3 and acts to compact chromatin and inhibit elongation through ubiquitylation of H2AK119. Thus, PRC1 has direct influence over transcriptional repression due to H3K27me3. Broader considerations include changes in the expression of the various histone modifying enzymes such as HATs, HMTs, HDACs, and HDMs as well as changes to transcription factors that mediate their recruitment to specific genes targets (Füllgrabe *et al.*, 2011). A third factor worth noting is that S3 cells treated acutely with vorinostat were under stress due to the cytotoxicity of vorinostat, particularly at 3 μM. The impact of cellular stress on gene expression and H3K27 modifications at the PRC2 targets investigated is unknown at this time.

4.2 Targeted Inhibition of HDACs 1, 2, and 3 May Be Sufficient to Produce the Non-Malignant Phenotype

Promising results were observed with CI-994 adapted cells, which showed reduced proliferation and colony formation relative to S3 cells. In particular, 12 μM CI-994 adapted cells showed a substantial reduction in colony formation that approaches the reductions seen with SSH1 and SH80 cells. These results suggest that targeted inhibition of HDACs 1, 2, and 3 may reduce tumorigenicity. A colony formation assay using methylcellulose, as well as a study of tumor xenograft formation in immunodeficient mice, needs to be performed to get a better characterization of the tumorigenicity of CI-994 adapted cells.

Selected PRC2 targets showed similar changes in mRNA expression in CI-994 adapted cells compared to SH80 cells, with the exception of *WT1*. These results indicate that inhibition of HDACs 1, 2, and 3 leads to altered expression of PRC target genes. Substantial changes in gene expression due to CI-994 adaptation were observed for *TSPAN8*, *STMN2*, and *EDN3*, further reinforcing the idea that these genes may be of particular importance to the non-malignant phenotype. However, it is important to note that no difference in gene expression was observed between 9 μM and 12 μM CI-994 adapted cells while there was a marked difference in colony formation between the two adaptations. As more PRC2 target genes are evaluated, genes that show a difference in expression between the two concentrations may also be of importance to reducing tumorigenicity.

In contrast to SH80 cells, CI-994 adapted cells showed no change in expression of the PRC2 target gene *WT1* and the non-PRC2 target gene *SNAI2*. Additionally, the non-PRC2 target *DKK4* displayed substantially smaller changes in expression in CI-994 adapted cells compared to SH80

cells. These preliminary results suggest that fewer genes are affected by targeted inhibition of HDACs 1, 2, and 3. Expression of *EZH2* and *SUZ12* was relatively unchanged by CI-994 adaptation, indicating that the changes observed at PRC2 target genes are not due to changes in RNA expression of the core components of the PRC2 complex. A western blot is needed to determine if there are any changes in *EZH2* or *SUZ12* protein levels or modifications.

4.3 Future Directions

Given the results with the 12 μM CI-994 adapted cells, this may be a promising route to identifying the set of changes necessary and sufficient to generate the non-malignant phenotype. It is worth exploring whether an increase in CI-994 concentration leads to a reduction in colony formation that matches the reduction seen with SH80 cells. Once the most effective concentration is determined, cell lines should be established and characterized for CI-994 resistant clones and long-term culture of adapted cells without CI-994. RNA sequencing could be performed to look more globally for changes that may be important to reducing tumorigenicity and to specifically look at changes in PRC2 target genes in both SH80 and CI-994-adapted cells. If the gene expression signature of PRC2 targets is upregulated in CI-994 adapted cells as seen with SH80 cells, then ChIP-sequencing of both cell lines could be used to characterize histone modifications controlled by the PcG and TrxG systems and their global responses to histone deacetylase inhibition.

As new HDAC inhibitors become available, it may be possible to selectively inhibit individual HDACs. This would allow the individual effects of HDACs 1, 2, and 3 to be separated and explored in more depth.

Appendix A: qPCR Primer Sequences

A.1 RT-qPCR Primer Sequences

The primer sets used for RT-qPCR are given in Table A1. All sequences are listed in the 5' to 3' direction. Primers were obtained from Integrated DNA Technologies.

Table A1. RT-qPCR primer sequences. All primer sequences were downloaded from qPrimerDepot (Cui *et al*., 2007).

Gene	Forward Primer Sequence	Reverse Primer Sequence
CYP24A1	CGT CGA AGA CTT GTA CAG CG	CAT TCT TCT GGA GAA GCC CA
DACH1	TCC TGG GAT AAT TCC ACC AA	TGT CCA TGC CCA GTT AGA GA
DKK4	GGA GCT CTG GTC CTG GAC TT	TCT GGT ATT GCA GTC CGT GT
EDN3	GCA CGT GCT TCA CCT ACA AG	GGA CAG TCC ATA GGG CAC C
EZH2	TTG TTG GCG GAA GCG TGT AAA ATC	TCC CTA GTC CCG CGC AAT GAG C
GAL	GTT TCA TGT CAT CTT CGG GC	AAG GAA AAA CGA GGC TGG AC
GATA6	GAA TTC GCC ACC ATG GCC TTG ACT GAC GGC GGC TG	TCT AGA CAA AAG CAG ACA CGA GTG GAG TGA G
RNF128	GCC GTC ATC TTT AAC TTC CC	CCT TTC AGA TTG CCG ATC AT
STMN2	GAT GTT GAT GTT GCG AGG TT	TCT GCA CAT CCC TAC AAT GG
SNAI2	CAG ACC CTG GTT GCT TCA A	TGA CCT GTC TGC AAA TGC TC
SUZ12	TGA AAG GAG AGC AAG AAT CTC A	GCA GGA CTT CCA GGG TAA CA
TBP	TCT GGG ATT GTA CCG CAG C	CGA AGT GCA ATG GTC TTT AGG
TSPAN8	GCA GGT GTG AGT GCC TGT AT	TCG TAC CCA TAT TGC TAA TGC
WT1	GAA ATG GAC AGA AGG GCA GA	GAC ACC GTG CGT GTG TAT TC

A.2 ChIP qPCR Primer Sequences

The primer sets used for ChIP qPCR are given in Table A2. All sequences are listed in the 5' to 3' direction. Primers were obtained from Integrated DNA Technologies.

Table A2. ChIP qPCR primer sequences. Primers were designed by Hsin-Ching Lin of the Rabson Laboratory, except where noted (*).

Gene	Forward Primer Sequence	Reverse Primer Sequence
*CYP24A1** (-189/-274)	GGG GCT ATG TTC GCT GGG	GGG CTT CGC ATG ACT TCC T
DACH1 (-173/-89)	CCG AGT TCC TGG TTG GAT AA	GAG CTC CGG AAA CTT GAA ATA C
EDN3 (-345/-241)	GGC GTG AGT CAA GAG TGT AAA	GGC TGA GGG AAA GAC ACA TT
GAL (-471/-551)	AGT GTA GAG GAC AGG TAA GAT GA	GGC TCA ATA TCA GAT GGG TTG A
GATA6 (-965 / -708)	CAT TTC CAG TCC CTT TTG CCC	TTC CAC ATC AGT CGT GTC CGA G
RNF128 (-103/-3)	TGC AGG AAG TCA TCC AAT CC	TGT ACA CAC AGG TAA CCC TTA AC
SNAI2 (-122/-32)	CTC CAG ATG CCA CTT CCA AAT A	TCC GCC AGG AGA AGG AA
STMN2 (-387/-276)	ATC CCT ATT CCC AAG CAA CC	CTG GAC TTA GGC GTC TCT AAA C
TSPAN8 (-434/-345)	GAT AGG GAA CAT TGG CAG TAG G	AAC CAT TTC CCA CAT ACC TCA A
WT1 (-588/-490)	GAC CTC TGG AAC CCA CAA AG	TTG AGT CTG GCT CTT GCT TC

Appendix B: ChIP Data as Percent Input

Table B1. ChIP data as % Input for H3K27me3, H3K27ac, and H3. Values are listed for all biological replicates (Rep 1, Rep 2, and Rep 3).

CYP24A1									
	% Input H3K27me3			% Input H3K27ac			% Input H3		
Cell Line	Rep 1	Rep 2	Rep 3	Rep 1	Rep 2	Rep 3	Rep 1	Rep 2	Rep 3
S3	0.039	0.124	0.131	2.387	5.544	4.442	0.375	1.057	0.656
1 µM - 96h	0.013	0.028	0.035	4.309	10.157	7.422	0.175	0.691	0.490
3 µM - 96h	0.005	0.026	0.014	3.965	9.102	4.323	0.405	0.531	0.356
SSH1	0.004	0.046	0.027	4.726	11.513	9.424	0.163	0.460	0.356
SH80	0.002	0.016	0.007	8.399	13.539	7.468	0.308	0.475	0.268
DACH1									
	% Input H3K27me3			% Input H3K27ac			% Input H3		
Cell Line	Rep 1	Rep 2	Rep 3	Rep 1	Rep 2	Rep 3	Rep 1	Rep 2	Rep 3
S3	0.095	0.207	0.193	1.309	1.545	1.389	0.393	0.640	0.449
1 µM - 96h	0.021	0.066	0.061	2.685	4.192	3.939	0.199	0.436	0.333
3 µM - 96h	0.007	0.011	0.015	3.616	5.492	4.613	0.288	0.391	0.257
SSH1	0.015	0.032	0.020	4.134	5.650	5.124	0.217	0.367	0.333
SH80	0.001	0.019	0.004	4.920	10.456	5.541	0.271	0.410	0.164
EDN3									
	% Input H3K27me3			% Input H3K27ac			% Input H3		
Cell Line	Rep 1	Rep 2	Rep 3	Rep 1	Rep 2	Rep 3	Rep 1	Rep 2	Rep 3
S3	0.048	0.229	0.161	1.369	2.920	2.335	0.390	1.183	0.640
1 µM - 96h	0.078	0.360	0.324	0.730	1.649	1.200	0.307	1.250	0.777
3 µM - 96h	0.097	0.257	0.264	1.602	2.671	1.921	0.890	1.230	0.800
SSH1	0.322	1.641	1.409	0.160	0.340	0.293	0.478	1.470	1.679
SH80	0.397	3.513	1.349	0.613	1.167	0.444	1.057	2.552	1.029

GAL									
	% Input H3K27me3			% Input H3K27ac			% Input H3		
Cell Line	Rep 1	Rep 2	Rep 3	Rep 1	Rep 2	Rep 3	Rep 1	Rep 2	Rep 3
S3	0.052	0.173	0.137	0.327	0.288	0.509	0.483	1.392	0.943
1 µM - 96h	0.071	0.314	0.185	0.286	0.516	0.566	0.373	1.228	0.824
3 µM - 96h	0.116	0.581	0.260	0.568	1.294	0.684	0.836	2.327	0.980
SSH1	0.140	0.699	0.507	0.301	0.588	0.416	0.614	1.658	1.253
SH80	0.216	1.508	0.723	0.247	0.637	0.321	1.199	2.751	1.222
GATA6									
	% Input H3K27me3			% Input H3K27ac			% Input H3		
Cell Line	Rep 1	Rep 2	Rep 3	Rep 1	Rep 2	Rep 3	Rep 1	Rep 2	Rep 3
S3	0.162	0.630	0.660	0.603	0.943	1.172	0.370	1.031	0.746
1 µM - 96h	0.013	0.043	0.037	2.479	5.098	5.962	0.227	0.651	0.555
3 µM - 96h	0.006	0.016	0.021	4.721	8.732	5.443	0.549	0.675	0.604
SSH1	0.004	0.033	0.045	3.081	7.211	6.643	0.292	0.515	0.553
SH80	0.001	0.025	0.004	6.719	12.232	4.725	0.478	0.866	0.237
RNF128									
	% Input H3K27me3			% Input H3K27ac			% Input H3		
Cell Line	Rep 1	Rep 2	Rep 3	Rep 1	Rep 2	Rep 3	Rep 1	Rep 2	Rep 3
S3	0.199	0.533	0.386	0.041	0.071	0.066	0.435	1.344	0.641
1 µM - 96h	0.104	0.403	0.312	0.191	0.271	0.237	0.304	0.807	0.675
3 µM - 96h	0.108	0.267	0.310	0.966	1.234	1.109	0.567	0.805	0.546
SSH1	0.058	0.329	0.127	0.238	0.454	0.210	0.397	1.204	0.583
SH80	0.037	0.356	0.127	0.228	0.850	0.262	0.761	2.948	1.294

SNAI2									
	% Input H3K27me3			% Input H3K27ac			% Input H3		
Cell Line	Rep 1	Rep 2	Rep 3	Rep 1	Rep 2	Rep 3	Rep 1	Rep 2	Rep 3
S3	0.003	0.014	0.017	2.835	4.548	5.022	0.174	0.600	0.315
1 µM - 96h	0.002	0.004	0.002	3.845	11.893	10.218	0.081	0.310	0.231
3 µM - 96h	0.001	0.004	0.004	5.633	14.883	10.518	0.262	0.405	0.360
SSH1	0.000	0.002	0.004	8.202	12.339	9.338	0.151	0.357	0.254
SH80	0.002	0.017	0.007	8.564	19.161	12.798	0.344	0.524	0.272
STMN2									
	% Input H3K27me3			% Input H3K27ac			% Input H3		
Cell Line	Rep 1	Rep 2	Rep 3	Rep 1	Rep 2	Rep 3	Rep 1	Rep 2	Rep 3
S3	0.415	1.227	0.862	0.029	0.045	0.04	0.716	1.462	1.00
1 µM - 96h	0.169	0.515	0.388	0.092	0.105	0.10	0.526	1.134	0.93
3 µM - 96h	0.076	0.272	0.212	0.614	0.914	0.68	0.756	1.139	0.66
SSH1	0.226	0.793	0.419	0.151	0.261	0.13	0.863	1.745	1.02
SH80	0.010	0.085	0.032	1.668	3.409	2.15	0.674	1.843	0.91
TSPAN8									
	% Input H3K27me3			% Input H3K27ac			% Input H3		
Cell Line	Rep 1	Rep 2	Rep 3	Rep 1	Rep 2	Rep 3	Rep 1	Rep 2	Rep 3
S3	0.493	1.182	1.020	0.065	0.069	0.103	0.409	1.116	0.733
1 µM - 96h	0.138	0.583	0.322	0.207	0.299	0.414	0.238	0.880	0.553
3 µM - 96h	0.093	0.261	0.268	1.144	1.622	1.454	0.574	0.620	0.533
SSH1	0.140	0.866	0.629	0.370	0.830	0.421	0.418	1.224	0.896
SH80	0.033	0.184	0.066	0.915	4.259	2.172	0.639	1.797	0.704

WT1									
	% Input H3K27me3			% Input H3K27ac			% Input H3		
Cell Line	Rep 1	Rep 2	Rep 3	Rep 1	Rep 2	Rep 3	Rep 1	Rep 2	Rep 3
S3	0.166	0.449	0.270	0.506	0.688	0.789	0.572	1.397	0.932
1 µM - 96h	0.148	0.411	0.337	0.615	0.847	0.904	0.483	1.345	0.966
3 µM - 96h	0.203	0.569	0.510	0.624	1.099	2.013	1.020	1.511	1.219
SSH1	0.243	0.811	0.511	0.871	1.065	0.862	0.858	1.479	1.133
SH80	0.254	1.952	0.782	1.023	2.297	1.112	1.242	2.453	1.078

References

1. Ahmed D, Eide PW, Eilertsen IA, Danielsen SA, Eknæs M, Hektoen M, Lind GE, Lothe RA. 2013. Epigenetic and genetic features of 24 colon cancer cell lines. Oncogenesis. 2: e71.

2. Beckers T, Burkhardt C, Wieland H, Gimmnich P, Ciossek T, Maier T, Sanders K. 2007. Distinct pharmacological properties of second generation HDAC inhibitors with the benzamide or hydroxamate head group. Int J Cancer. 121(5): 1138-48.

3. Berger SL. The complex language of chromatin regulation during transcription. 2007. Nature. 447(7143): 407-12.

4. Berger SL, Kouzarides T, Shiekhattar R, Shilatifard A. 2009. An operational definition of epigenetics. Genes Dev. 23(7): 781-3.

5. Bolden JE, Peart MJ, Johnstone RW. 2006. Anticancer activities of histone deacetylase inhibitors. Nat Rev Drug Discov. 5(9): 769-84.

6. Cui W, Taub DD, Gardner K. 2007. qPrimerDepot: a primer database for quantitative real time PCR. Nucleic Acids Res. 35(Database issue): D805-9.

7. Dawson MA, Kouzarides T. 2012. Cancer epigenetics: from mechanism to therapy. Cell. 150(1): 12-27.

8. Deb G, Singh AK, Gupta S. 2014. EZH2: not EZHY (easy) to deal. Mol Cancer Res. 12(5): 639-53.

9. Füllgrabe J, Kavanagh E, Joseph B. 2011. Histone onco-modifications. Oncogene. 30(31): 3391-403.

10. Hock H. 2012. A complex Polycomb issue: the two faces of EZH2 in cancer. Genes Dev. 26(8): 751-5.

11. Højfeldt JW, Agger K, Helin K. 2013. Histone lysine demethylases as targets for anticancer therapy. Nat Rev Drug Discov. 12(12): 917-30.

12. Iyer NG, Ozdag H, Caldas C. 2004. p300/CBP and cancer. Oncogene. 23(24): 4225-31.

13. Kelly WK, Richon VM, O'Connor O, Curley T, MacGregor-Curtelli B, Tong W, Klang M, Schwartz L, Richardson S, Rosa E, Drobnjak M, Cordon-Cordo C, Chiao JH, Rifkind R, Marks PA, Scher H. 2003. Phase I clinical trial of histone deacetylase inhibitor: suberoylanilide hydroxamic acid administered intravenously. Clin Cancer Res. 9(10 Pt 1): 3578-88.

14. Kolybaba A, Classen AK. 2014. Sensing cellular states--signaling to chromatin pathways targeting Polycomb and Trithorax group function. Cell Tissue Res. 356(3): 477-93.

15. Kouzarides T. 2007. Chromatin modifications and their function. Cell. 128(4): 693-705.

16. Ma X, Ezzeldin HH, Diasio RB. 2009. Histone deacetylase inhibitors: current status and overview of recent clinical trials. Drugs. 69(14): 1911-34.

17. Markert EK, Mizuno H, Vazquez A, Levine AJ. 2011. Molecular classification of prostate cancer using curated expression signatures. Proc Natl Acad Sci USA. 108(52): 21276-81.

18. Mills AA. 2010. Throwing the cancer switch: reciprocal roles of polycomb and trithorax proteins. Nat Rev Cancer. 10(10): 669-82.

19. Morey L, Helin K. 2010. Polycomb group protein-mediated repression of transcription. Trends Biochem Sci. 35(6): 323-32

20. Oliver SS, Denu JM. 2011. Dynamic interplay between histone H3 modifications and protein interpreters: emerging evidence for a "histone language". Chembiochem. 12(2): 299-307.

21. Schuettengruber B, Martinez AM, Iovino N, Cavalli G. 2011. Trithorax group proteins: switching genes on and keeping them active. Nat Rev Mol Cell Biol. 12(12): 799-814.

22. Smith E, Lin C, Shilatifard A. 2011. The super elongation complex (SEC) and MLL in development and disease. Genes Dev. 25(7): 661-72.

23. Squazzo SL, O'Geen H, Komashko VM, Krig SR, Jin VX, Jang SW, Margueron R, Reinberg D, Green R, Farnham PJ. 2006. Suz12 binds to silenced regions of the genome in a cell-type-specific manner. Genome Res. 16(7): 890-900.

24. Steffen PA, Ringrose L. 2014. What are memories made of? How Polycomb and Trithorax proteins mediate epigenetic memory. Nat Rev Mol Cell Biol. 15(5): 340-56.

25. Ullius A, Lüscher-Firzlaff J, Costa IG, Walsemann G, Forst AH, Gusmao EG, Kapelle K, Kleine H, Kremmer E, Vervoorts J, Lüscher B. 2014. The interaction of MYC with the trithorax protein ASH2L promotes gene transcription by regulating H3K27 modification. Nucleic Acids Res. 42(11): 6901-20.

26. van der Vlag J, Otte AP. 1999. Transcriptional repression mediated by the human polycomb-group protein EED involves histone deacetylation. Nat Genet. 23(4): 474-8.

27. Witt O, Deubzer HE, Milde T, Oehme I. 2009. HDAC family: What are the cancer relevant targets? Cancer Lett. 277(1): 8-21.

28. Yoo KH, Hennighausen L. 2012. EZH2 methyltransferase and H3K27 methylation in breast cancer. Int J Biol Sci. 8(1): 59-65.